Microtubule association of TRIM3 revealed by differential extraction proteomics

Hannah L. Glover[1,4], Marta Mendes[2], Joana Gomes-Neto[1], Emma V. Rusilowicz-Jones[1], Daniel J. Rigden[1], Gunnar Dittmar[2,3], Sylvie Urbé[1*], Michael J. Clague[1*]

[1]Dept. of Biochemistry Cell and Systems Biology, ISMIB, University of Liverpool, Liverpool, L69 3BX, UK.
[2]Proteomics of Cellular Signalling, Department of Infection and Immunity, Luxembourg Institute of Health
[3]Department of Life Sciences and Medicine, University of Luxembourg, 2 avenue de l'Université, Campus Belval, L-4365 Esch-sur-Alzette, Luxembourg
[4]Current address: Cancer Research UK Beatson Institute, Switchback Road, Glasgow G61 1BD, U.K.

* corresponding authors clague@liverpool.ac.uk, urbe@liverpool.ac.uk

Key words: microtubules, proteomics, Nocodazole, Taxol, TRIM proteins

Abstract

The microtubule network is formed from polymerised Tubulin subunits and associating proteins, which govern microtubule dynamics and a diverse array of functions. To identify novel microtubule binding proteins, we have developed an unbiased biochemical assay which relies on the selective extraction of cytosolic proteins from cells, whilst leaving behind the microtubule network. Candidate proteins are linked to microtubules by their sensitivities to the depolymerising drug Nocodazole or the microtubule stabilising drug, Taxol, which are then quantitated in a triplexed mass spectrometry experiment. Our approach is benchmarked by co-segregation of Tubulin and previously established microtubule-binding proteins. We then identify several novel candidate microtubule binding proteins. Amongst these, we have selected the ubiquitin E3 ligase TRIM3 (Tripartite motif-containing protein 3) for further characterisation. TRIM3 binding to microtubules is mapped to its C-terminal NHL-repeat region. We show that TRIM3 is required for the rapid accumulation of acetylated Tubulin, following treatment with the microtubule stabilising drug Taxol. Furthermore, loss of TRIM3, partially recapitulates the reduction in nocodazole-resistant microtubules characteristic of Alpha-Tubulin Acetyltransferase 1 (ATAT1) depletion. These results can be explained by a decrease in ATAT1 following depletion of TRIM3 that is independent of transcription.

Introduction

Microtubules are formed from α- and β-Tubulin heterodimer subunits which polymerise to form hollow fibres, making up one of three major cytoskeletal elements [1]. They are polar structures, defined by a growing plus-end towards the cell periphery and a minus-end which is usually stabilised at the microtubule organising centre (MTOC) [2]. Microtubule (MT) networks are able to grow and shrink via continuous rounds of polymerisation and depolymerisation, allowing for constant cytoskeleton remodelling derived from their dynamic instability [3]. Consequently, they contribute to a wide variety of cellular functions such as maintaining cell shape, cell movement, cell division and provide the main structural unit for flagella and cilia [4]. They also provide tracks, along which motor proteins can travel, to distribute their cargo such as organelles and membranous vesicles [5, 6].

Numerous microtubule associated proteins (MAPs) account for this diverse array of functions. Some specifically bind to the end of microtubules to either control their attachment to cellular structures (-end) or their dynamics (+end). The first MAPs were discovered during the development of protocols for Tubulin purification [7, 8]. Similarly, the protein Tau was identified from porcine brain extracts, as a factor governing microtubule polymerisation [9]. Modern LC-MS/MS techniques provide a large scale, global and unbiased method for identifying MAPs. Prior MAP-centric proteomic studies have been performed using a variety of species. Over 250 MAPs were identified from early Drosophila embryos using Taxol- and GTP-stabilised endogenous Tubulin preparations, followed by 2D gel electrophoresis [10]. In a separate study, macrophage extracts were incubated with the microtubule stabilising drug Taxol and purified bovine brain Tubulin, with candidate MAPs being identified by spectral counting [11]. In 2010, more than 300 proteins from meiotic *Xenopus* egg extracts were found to bind to Taxol-stabilised bovine brain Tubulin [12]. A final example identified over 1000 proteins binding *in vitro* to the metaphase spindle isolated from CHO cells, using Multi-dimensional Protein Identification Technology [13].

The majority of these studies preceded major advances in the sensitivity of mass spectrometry instruments and the adoption of isotopic labelling procedures (e.g. SILAC, DML, TMT) that provide more quantitative data. Furthermore, many involve the manipulation of the microtubule network *in vitro* and/or the addition of

exogenous Tubulin, thereby incompletely capturing the intracellular architecture and environment. In this study, we take a different approach, by identifying the proteins that remain bound to a residual microtubule network, assembled under physiological conditions, following the extraction of cytosol. We have conducted a triplexed mass spectrometric analysis, which quantitates the sensitivity of mild detergent protein extraction from USOS cells, to prior manipulation of the network by microtubule depolymerising (Nocodazole) or stabilising (Taxol) drugs. We describe the development of this methodology and the general features of our results. Our analysis revealed several novel candidate microtubule binding proteins including the ubiquitin E3-ligase, TRIM3 (Tripartite motif-containing protein 3), for which we present a detailed characterisation of its association and effect on microtubule properties.

Results and discussion

Optimisation of the microtubule extraction protocol

Our initial approach involved an iteration of a previously described method to extract microtubule-associated proteins directly from U2OS cells [14]. A buffer which lyses cells whilst maintaining microtubules (Lysis and Microtubule Stabilisation buffer, LMS), is added to remove cytosolic proteins and small molecules, including any free Tubulin present. Vehicle-treated cells are depleted of cytosol, whereas the intact microtubules and MAPs are retained. For comparison, we used a condition pre-treated with the microtubule depolymerising drug Nocodazole, which provides us with a microtubule-depleted fraction. We first optimised the Nocodazole incubation conditions required to achieve maximum microtubule depolymerisation. U2OS cells were treated with increasing concentrations up to 12 μM and varying times at 37°C (Figure 1A, B). On this basis we selected a concentration of 6 μM for one hour as the optimal treatment although a minor fraction of microtubules remained resistant to depolymerisation. Rather than use high calcium conditions to release microtubules after cytosol extraction as described by Duerr et al. [14], we have simply lysed the cell remnants with 8 M urea lysis buffer. By labelling each condition with amino acids bearing

different stable isotopes, remaining non-microtubule related proteins are simply discounted by virtue of their 1:1:1 ratios, which are determined from subsequent mass spectrometry analysis. Prior to a large scale mass spectrometry analysis, we checked that the established MAPs, EML4 and MAP4, demonstrated the expected behaviour by Western blotting and immunofluorescence respectively (Figure 1C, D). A schematic of the fully optimised protocol is shown in Figure 1E.

Determination of the microtubule proteome

To determine the microtubule associated proteome via quantitative mass spectrometry, we generated extracts from SILAC (Stable Isotope Labelling with Amino acids in Cell culture) labelled U2OS cells subjected to 3 different scenarios, control or prior treatment with Nocodazole and Taxol respectively (Figure 1E). The 3 residual fractions were combined in a 1:1:1 ratio. The $\log_2$ transformed ratio of Nocodazole/Control values were ranked from the highest score to the lowest. To confirm microtubule enrichment and define a cut-off point for further analysis, hits were analysed in sequential groups of 10 (1-10, 2-11....) for their enrichment score for 'microtubule' or 'microtubule-binding' using DAVID Bioinformatics Resource 6.8 until no enrichment was observed for 10 consecutive groups (Figure 2A) [15]. The distribution of the normalised Nocodazole/Control ratio (x-axis) versus the normalised Taxol/control ratio (y-axis) is shown in Figures 2B and C. Proteins represented by data points in the top left quadrant of this graph, will have been lost due to Nocodazole treatment and preferentially retained following Taxol treatment. The plotted ratios derive from averaging across constituent peptides of any given protein. The behaviour of each individual peptide from selected proteins is represented in Figure S1A. Figure S1B shows a heat map of outlying Nocodazole sensitive proteins across 3 independent repeats.

As expected the strongest outliers in terms of Nocodazole sensitivity are 12 isotypes of Tubulin (Figure 2B). With one exception, TUBB8, these are enriched by Taxol treatment. The known microtubule associated protein, MAP4, clusters with these Tubulin isoforms alongside the poorly characterised DPYSL2 (Dihydropyriminidase like 2), otherwise known as Collapsin response mediator protein-2 (CRMP-2), which mediates the addition of Tubulin to the positive end of the growing microtubule [16]. We were surprised to find Galectin-related protein

(LGALSL), to be so strongly aligned with this cluster. This small protein is a candidate amyotrophic lateral sclerosis (ALS) gene, which contains a Galectin domain, although most of the residues critical for carbohydrate binding are not conserved [17]. Expression of GFP-LGALSL in U2OS cells shows a Nocodazole-dependent microtubule association that is highly prominent following LMS-mediated extraction of cytosol (Figure S2A).

Moving to the bottom left quadrant of Figure 2B, we will find proteins that are lost upon both Nocodazole and Taxol treatments i.e. those that associate with dynamically unstable microtubules. This is exemplified by the strong outlier MAPRE3 (Microtubule Associated Protein RP/EB Family Member 3) otherwise known as EB3, a plus-end tracking protein (+TIP) that binds to the plus-end of microtubules and regulates the dynamics of the microtubule cytoskeleton. Note, a further Collapsin response mediator protein, DPYSL3 appears in this quadrant. Thus, DPYSL2 and 3 show similar sensitivities to Nocodazole but are differentiated by their response to Taxol. MT minus-ends that are not attached to the centrosome are stabilised by calmodulin-regulated spectrin-associated 2 (CAMSAP2, sensitive to Nocodazole only, Figure 2B), and many of them are tethered to the Golgi apparatus [18]. Loss of MAPRE3 leads to shortening of CAMSAP2-decorated MT minus-end stretches, their detachment from the Golgi, and Golgi compaction [19].

To identify novel microtubule candidate proteins we next inspected the group of proteins de-enriched by Nocodazole treatment, that are clearly separated from the main cloud of data-points and falling within our cut-off. These include the ALS associated gene, regulator of microtubules dynamics protein 3 (RMDN3), otherwise known as PTPIP51, which shows particular sensitivity to Taxol. This is annotated as a mitochondrial localised protein and known to regulate ER-mitochondrial association [20]. Co-segregation of proteins across both dimensions can be used to infer association and it is interesting that the nearest neighbour of RMDN3 in our data-set is a component of the outer mitochondrial sorting and assembly machinery, SAMM50 that is critical for mitochondrial organisation [21]. Thus two mitochondrial membrane bound proteins are amongst the most sensitive proteins to Taxol treatment. Their presence is anomalous and not reflective of mitochondrial proteins generally. Alongside the mitochondrial inner membrane protein CKMT1A, these two are the only integral membrane proteins amongst the

outlying group. We also find the ubiquitin E3 ligase family member Tripartite Motif Containing 3 (TRIM3) firmly within this quadrant, for which we provide a detailed characterisation below.

We were surprised to find a coherent group of proteins in the top right hand quadrant (Figure 2C) i.e. enriched by both Nocodazole and Taxol treatments. This group contains multiple subunits from the cytoplasmic dynein and dynactin complexes: the minus-end directed microtubule motor protein and its essential cofactor respectively [22, 23]. Bicaudal D2 (BICD2) is an adaptor protein, which recruits dynein and stabilises the interaction between dynein and dynactin. Platelet Activating Factor Acetylhydrolase 1b Regulatory Subunit 1 (PAFAH1B1, also known as LIS1), is required for dynein-mediated transport and accumulation of dynein at microtubule plus-ends [24]. Finally, Actin Related Protein 10 (ACTR10) has been shown to induce dynein and dynactin interaction [25]. Confirmatory results by Western blotting for cytoplasmic dynein 1 light intermediate chain 1 (DYNC1LI1) are shown in Figure S2B. When looked at by immunofluorescence we can see that Nocodazole treatment leads to a translocation of DYNC1LI1 to the nuclear membrane, which is retained upon LMS extraction (Figure S2C). This Nocodazole-induced translocation phenomenon has been previously described for dynein, and reflects conditions in the G2 phase of the cell cycle leading to association of BICD2 and dynein with nuclear pores [26, 27].

TRIM3: a novel microtubule binding protein

As detailed above, TRIM3, otherwise known as BERP, is clearly identified as an outlier protein, that is de-enriched by both Taxol and Nocodazole treatments. The Nocodazole sensitivity is confirmed by Western blots showing the corresponding extraction pattern (Figure 3A). It belongs to the TRIM family of E3 ligases, some of which have been previously localised to microtubules [28]. Up until now, microtubule association has been confined to TRIM proteins that possess a COS motif, FNIII and SPRY/B30.2 domain as their C-terminal domain arrangement [29, 30]. To determine whether TRIM3 is truly a novel MAP, mouse GFP-TRIM3 was transiently transfected into U2OS cells and co-stained for α-Tubulin, showing a clear co-localisation. This typical distribution is lost upon Nocodazole treatment but remains evident with Taxol (Figure 3B). Thus, we have been able to use our

proteomics approach to identify a second novel MAP alongside LGALSL reported above.

Microtubules are highly decorated with a large number of post-translational modifications (PTMs), and it has come to light that these modifications can play a role in directing which MAPs can associate with which microtubule subsets [31]. Therefore we analysed whether TRIM3 colocalises with a particular microtubule subset. Figures 3C illustrates that GFP-TRIM3 localises to all microtubule subsets and is not specific to either detyrosinated or acetylated microtubules. However, TRIM3 does not associate with the centrosome (Figure 3D). The microtubule network undergoes major redistribution during mitosis. Following the behaviour of TRIM3 though mitosis in synchronised cells, we observed GFP-TRIM3 on the mitotic spindle from metaphase right through to telophase (Figure 3E, Supplementary Movie 1). The closest paralogue to TRIM3 is TRIM2 and GFP-TRIM2 also shows a clear microtubule association which has not hitherto been reported (Figure S3).

The C-terminal region is responsible for TRIM3 localisation to microtubules

TRIM family proteins are defined by their common domains at their N-terminal end and are divided into subfamilies based on their C-terminal domains. Several of these proteins have been previously described to localise to microtubules via a signature amino acid sequence, named the COS box, which follows the coiled-coil domain [29]. Mutations induced at the beginning and end of this region lead to dissociation from the microtubule network. A schematic and AlphaFold 2 derived structural model of TRIM3 are shown in Figures 4A and B respectively, illustrating the family specific tripartite motif (RING, BB2, Coiled-coil) followed by a short α-helix, a filamin domain and NHL-repeats. Sequence alignments of human TRIM family members reveal that the conserved amino acids within the COS-box, shown to be required for microtubule localisation, are not present within TRIM3 or TRIM2. This suggests that microtubule network localisation is achieved by other means (Figure S4). Inspection of the 3D structures of TRIM proteins predicted by AlphaFold 2 revealed that all COS-box proteins as well as TRIM3 contain a short α-helix structure shortly after the coiled-coil domain (Figure 4B).

In order to map which region of TRIM3 is required for microtubule localisation, nine different GFP-tagged truncation or deletion constructs were

generated (Figure 4C). Removal of the tripartite motif does not affect microtubule localisation: truncations comprising the helix, filamin and NHL-repeats in isolation are still able to successfully colocalise with Tubulin. Concordantly the N-terminal TRIM motif-only construct does not bind microtubules. The C-terminal region is therefore responsible for microtubule binding. Further analysis of the constructs implicate the C-terminal NHL-repeat region as the primary determinant of microtubule binding (Figure 4C,D).

Taxol and Nocodazole treatments reveal an influence of TRIM3 on microtubule properties

We next sought to define a role for TRIM3 in relation to microtubule network properties. TRIM3 was efficiently depleted using siRNA transfection, and immunoblotting and immunofluorescence analyses were performed. Figure 5A confirms that levels of total Tubulin, acetylated Tubulin or detyrosinated Tubulin are unchanged following depletion for all indicated time frames. Visual inspection and quantitative analysis does not reveal any obvious perturbation of the microtubule network (Figure 5B, Figure S5A). Microtubule networks that are stabilised with acute Taxol treatment undergo an increase in detyrosination and acetylation. To determine whether TRIM3 plays a role in accumulation rate of these microtubule modifications, TRIM3 was depleted for 72 h before treating with Taxol over a 60 minute period. Quantification from three independent repeats reveals that accumulation of detyrosination is not significantly affected, however acetylation is unable to further accumulate under these conditions despite starting from identical baseline levels (Figure 6A,B). Acetylation is a marker of long-lived microtubules, and has previously been shown to be involved in protecting microtubules from mechanical ageing [32, 33]. Depletion of the enzyme responsible for microtubule acetylation, Alpha-Tubulin Acetyltransferase 1 (ATAT1) leads to changes in the Nocodazole resistant fraction of microtubules, a finding we have reproduced here (Figure 6C) [33]. Correspondingly, we find that TRIM3 depletion partially reproduces this phenotype, wherein residual microtubules are clearly sparser. Thus, by orthologous approaches, we have been able to link TRIM3 to ATAT1 dependent properties of microtubules. This influence of TRIM3 can be accounted for by a reduction ATAT1 levels upon TRIM3 depletion, which is not due to effects upon transcription as mRNA levels are unchanged (Figure 6D, E). How this mechanism is effected is currently unclear. ATAT1 is a relatively stable protein

(Figure S5B) and any direct TRIM3 enzyme-substrate relationship would be expected to result in an increase in ATAT1 levels upon TRIM3 depletion, rather than the observed decrease. Additionally, TRIM3 is a relatively poor E3 ligase in isolation, but can be activated by association with its paralogue TRIM2 [34]. Note that although we also show microtubule association of TRIM2, we do not detect it in our proteomic analysis. At this point we cannot rule out TRIM3-mediated effects upon ATAT1 translation, particularly as its NHL repeat domain is proposed to confer RNA binding activity as well as the MT-binding shown here [35].

In summary, we have established a new method for identification of MAPs which we hope will translate into other cell types and prove useful in the investigation of pathological conditions. The ability to culture iPSC neurons at scale may offer an opportunity to transfer our system to a specialised microtubule network. Our vision is that this method will be one component of a new wave of mass spectrometry based methods to comprehensively detail the MAPome. There is a broad unresolved question as to why so many TRIM family ubiquitin E3 ligases associate with microtubules, to which we now contribute two new examples. TRIM2 has been previously linked to neuronal polarisation and knock-out mice show evidence of neurodegeneration [36, 37]. TRIM3 has been shown to associate with the neuron-specific kinesin KIF21B [38]. TRIM2 and TRIM3 are both enriched in the brain and their functions there must be considered in the light of our findings.

Materials and Methods

Cell culture

U2OS cells from European Collection of Authenticated Cell Cultures (ECACC) were grown in Dulbecco's Modified Eagle Medium (DMEM) supplemented with 10% heat-inactivated foetal bovine serum. Cells were cultured at 37 °C with 5% CO_2 and split every 2-3 days at 1:4 or 1:5 dilutions.

Antibodies

The following primary antibodies were used for western blotting at the respective concentrations: α-Tubulin (Sigma, T5168, 1:10,000), acetylated α-Tubulin (Sigma,

T6793, 1:1000), ATAT1 (Proteintech, 28828-1-AP, 1:500), Detyrosinated α-Tubulin (Abcam, ab32386, 1:1000), DYNC1LI1 (Atlas, HPA035013, 1:1000), EML4 (Cell Signaling Technology, 12156S, 1:1000), GAPDH (Cell Signalling Technology, 2118S, 1:1000). The following primary antibodies were used for immunofluorescence at the respective concentrations: α-Tubulin (Bio-rad, MCA77G, 1:500), β-Tubulin (Abcam, ab6046, 1:200), acetylated α-Tubulin (Sigma, T6793, 1:1000), Detyrosinated α-Tubulin (Abcam, ab32386, 1:200), DYNC1LI1 (Atlas, HPA035013, 1:1000), MAP4 (Bethyl, A301-488A, 1:1000), Pericentrin (Abcam, ab4448, 1:1000). Secondary antibodies used for western blotting obtained from LICOR Biosciences: Donkey anti-mouse IRDYE 800CW (926-32212), Donkey anti-mouse IRDYE 680CW (926-32222), Donkey anti-rabbit IRDYE 800CW (926- 32213), Donkey anti-rabbit IRDYE 680CW (926-32223). Secondary antibodies used for immunofluorescence obtained from Invitrogen: Donkey anti-rabbit AF488 (A21206), Donkey anti-rabbit AF594 (A21207), Donkey anti-mouse AF488 (A21202), Donkey anti-mouse AF594 (A21203), Donkey anti-rat AF594 (A21209).

Plasmids

Full length LGALSL was amplified by PCR from pBluescriptR-LGALSL purchased from Horizon Discovery (Cambridge, UK) (MHS6278-202809144, clone ID: 5301908). Full length TRIM2, mTRIM3 and mTRIM3 truncations and deletions were amplified by PCR from pcDNA3X(+)MycEGFP-TRIM2 and pcDNA3X(+)MycEGFP-mTRIM3 which were a kind gift from Prof. Germana Meroni (University of Trieste). PCR amplicons were then sub-cloned into BglII and SalI sites of the pEGFP-C1 vector.

Drug treatments

All drug treatments were carried out in normal culture medium. Nocodazole was used at 330 nM for synchronisation and 6 μM for microtubule depolymerisation. Taxol was used at 6 μM for microtubule stabilisation and 600 nM for accumulation of modifications. Thymidine was used at 2 mM and cycloheximide at 100 μg/ml. The duration of treatments is detailed in respective figure legends.

Cell lysis, SDS-PAGE and Western blotting

Cells were placed on ice, rinsed twice with ice-cold PBS and lysed in RIPA buffer (150 mM NaCl, 1% Triton-X100, 0.1% SDS, 1% sodium deoxycholate, 10 mM Tris-HCL pH 7.5) supplemented with mammalian protease inhibitors (1:250 v/v) on a rocker on ice for 15 minutes. All samples were suspended in Laemmli sample buffer, boiled (95 °C, 5 minutes) and either used straight away or retained at -20 °C until required. 10-20 µg protein (unless stated) was resolved on precast NuPAGE Novex 4-12% Bis-Tris Gels in 3-(*N*-morpholino)propanesulfonic acid (MOPS) buffer (*Invitrogen*). Samples were transferred to 0.45 *µ*m nitrocellulose membrane (0.9 A, 1 h) in transfer buffer (0.2 M Glycine, 25 mM Tris, 20% methanol). Membranes were incubated in blocking solution (Tris buffered saline (TBS: 150 mM NaCl, 10 mM Tris, pH 7.5) supplemented with 0.1% Tween-20 (TBST, v/v), and 5% Marvel (w/v) for 1 h to prevent non-specific binding of antibodies. Membranes were incubated overnight with primary antibodies, washed 3X for 5 min in TBST before incubating in either IRDye-conjugated anti-mouse or anti-rabbit secondary antibodies in blocking solution for 1 h (1:15,000 v/v, *LI-COR*). LI-COR Odyssey Imaging Software was used at 800 nm or 680 nm for visualisation. Band intensities were quantitated using ImageStudio Lite. For quantitation across multiple experiments, raw values were either normalized to the sum of the raw values from each individual blot (Figure 5A and 6B) or normalised to the corresponding Actin bands (Figure 6D).

Fluorescence microscopy

Cells were seeded onto 22 mm^2 coverslips in 6-well plates and cultured overnight. They were then fixed with ice cold methanol (MeOH) at -20 °C for 5 min and washed in PBS before non-specific sites were blocked using 10% goat serum in PBS for 30 min at room temperature. Primary antibodies (1 h) and secondary antibodies (30 min) were applied sequentially in 5% goat serum, each followed by two 4 min washes with PBS. Coverslips were finally washed in water and mounted onto glass slides using Mowiol supplemented with DAPI. Images were acquired using either a Nikon Eclipse Ti microscope with a CFI Plan Apo 40x objective or a CFI Plan Apochromat VC 60X objective lens, or a 3i Marianas spinning disk confocal microscope (3i Intelligent Imaging innovations, Germany) with a Plan-Apochromat 40x/1.3NA Oil Objective or a Plan-Apochromat 63x/1.4NA Oil Objective M27 or

using a Zeiss LSM900 with Airyscan confocal laser scanning microscope using a 63x x 1.4 NA Zeiss Plan Apochromat objective.

Microtubule extraction protocol

Cells were treated with 6 µM of Nocodazole for 1 h or 6 µM of Taxol for 30 min at 37 °C alongside a DMSO control of equivalent volume. The following steps were either performed in a water bath at 37 °C using buffers which were preheated to 37 °C, or on ice using buffers pre-cooled to 4 °C. Cells were washed in PBS before being incubated in Lysis and Microtubule Stabilisation buffer (LMS: 100 mM PIPES pH 6.9, 5 mM $MgCl_2$, 1 mM EGTA, 30% glycerol, 0.1% NP40, 0.1% Triton X-100, 0.1% Tween-20, 0.1% 2-mercaptoethanol (v/v)) supplemented with MPIs (1:250) for 5 min and samples were collected. The remaining microtubules on the plates were then extracted using 8 M urea, 50 mM Tris, pH 8.

siRNA transfection

All siRNA treatments were performed the day after cell seeding. All siRNA protocols were performed using Lipofectamine RNAiMAX transfection reagent, in accordance with the manufacturer's protocol. Cells were seeded the day before treatment and 40 nM of siRNA was transfected. Cells were incubated for either 48 h or 72 h as specified. Sequences of siRNA oligos used are as follows: ONTARGETplus Non-targeting siRNA oligo#1 (NT1) 5'-TGGTTTACATGTCGACTAA-3' (Dharmacon, D-001810-01), TRIM3 oligo#1 GUACAGCACAGGCGGCAAA, oligo#2 GCACAUAUGAGCUAGUGUA, oligo#3 GAGCGCCACUGCACACGAA, oligo#4 GAAUGAAAUUGUAGUAACG (Dharmacon, L-006931-00), ATAT1 oligo#1 GUAGCUAGGUCCCGAUAUA, oligo#2 GAGUAUAGCUAGAUCCCUU, oligo#3 GGGAAACUCACCAGAACGA, oligo#4 CUUGUGAGAUUGUCGAGAU.

Plasmid DNA transfection

All plasmid DNA transfections were performed using Genejuice or Lipofectamine 2000 the day prior to collection of experimental data into either a 6-well plate or *µ*-Dish 35 mm high Ibidi® dishes (Ibidi LCC, Martinsried, Germany) for live cell imaging, with cells at 60-80% confluency at the time of transfection.

Cell synchronization and live cell imaging

For imaging of TRIM3 on the mitotic spindle, cells were synchronized to increase the mitotic index. Cells were seeded into 35 mm ibidi dishes the day prior to synchronization. Cells were synchronised at prometaphase using 2 mM thymidine (24 h) followed by 330 nM Nocodazole (16 - 18 h). Transfection with plasmid DNA was performed alongside Nocodazole addition. To allow cells to re-enter mitosis, cells were washed in fresh DMEM 3x before being incubated for 1 h prior to imaging. Cells in late prometaphase or metaphase were selected and z-stacks were acquired every minute as cells passed through mitosis. Imaging was acquired using a 3i Marianas spinning disk confocal microscope (3i Intelligent Imaging innovations, Germany) with a Plan-Apochromat 63x/1.4NA Oil Objective M27.

Analysis of stable microtubules

U2OS cells were transfected with siRNA against TRIM3 and ATAT1 alongside a non-targeting control (NT1) for 72 h. Cells were then treated with 6 μM Nocodazole for 1 h to depolymerise the dynamic microtubules whilst maintaining Nocodazole-resistant ones. Cells were washed twice in a buffer containing PIPES, HEPES, EGTA and $MgSO_4$ (PHEM: 60 mM PIPES, 25 mM HEPES, 10 mM EGTA and 4 mM Mg SO_4) before treating cells with PHEM buffer containing 0.2% Triton-X 100 for 1 min. This removes the cytosolic Tubulin (depolymerised microtubules) whilst maintaining the intact stable microtubules. Cells were then fixed and stained as described.

SILAC labelling

U2OS cells were cultured under standard conditions in DMEM for SILAC supplemented with 10% dialysed FBS and L-proline, Pro0 (200 µg/ml) to prevent conversion of arginine to proline. Differentially labelled amino acids were added to the media to generate SILAC media for 3 conditions: Light (L-lysine, Lys0; L-arginine, Arg0), Medium (L-lysine-$^{2}H_4$, Lys4; L-arginine-$^{13}C_6$, Arg6) and Heavy (L-lysine-$^{13}C_6$-$^{15}N_2$, Lys8; L-arginine-$^{13}C_6$-$^{15}N_4$, Arg10). L-lysine was supplemented at a final concentration of 146 µg/ml whereas L-arginine was supplemented at a final concentration of 84 µg/ml. Cells were cultured for a minimum of 6 passages and tested to confirm amino acid incorporation before experiments proceeded.

Extracted microtubules from each condition were combined at a 1:1:1 ratio and filtered through 15ml Amicon ultra centrifugal filters (10,000) at 4000g at RT until

the minimum volume was retained. The flow-through was discarded and the sample suspended in sample buffer before being subjected to processing for mass spectrometry.

Mass spectrometry

SDS-PAGE was performed until proteins had migrated 1/3 through the gel, then stained with Coomassie Blue. The sample lane was cut into 12 equal slices, then into 1 mm cubes and destained using 50 mM Ammonium bicarbonate (Ambic) containing 50% Acetonitrile (ACN, v/v) at 37°C in an Eppendorf ThermoMixer Compact at 900 rpm. Samples were dehydrated (ACN, 5 min) and dried via Speedvac rotary evaporation. Peptides were reduced in 10 mM dithiothreitol (56 °C, 1 h), alkylated in 55 mM iodoacetamide (RT, 30 min), washed in 100mM Ambic (15 min) then repeated in 50 mM Ambic with 50% ACN. Samples were dehydrated in ACN, followed by Speedvac evaporation. Peptides were cleaved with 3 µg trypsin per sample lane in 40 mM Ambic and 9% ACN (37 °C, overnight) then extracted using ACN (30°C, 30 min), followed by 1% formic acid (FA room temperature, 20 min) and then ACN again. Supernatants were dried in a Speedvac overnight and stored at -20°C until analysis.

Samples were desalted using C18 tips [39]. Briefly, samples were resuspended in 50 μl 0.1% FA. C18 tips were first activated with Methanol, equilibrated twice with 0.1% FA, then samples were loaded, and peptides were washed with 0.1% FA. Samples were then eluted with 80% ACN / 0.1% FA and dried in the speed vac. Finally, they were reconstituted in 0.1% FA. Peptides were then fractionated on a QExactive HF plus column coupled to a nanoHPLC Ultimate 3000 using a pre-concentration onto a nano-column configuration. An Acclaim PepMap 100 (75 μm, 2 cm) was used to do the pre-concentration and an Acclaim PepMap RSLC (Rapid separation liquid chromatography, 75 μm, 15 cm) was used for peptide separation. Total run time was 118 min with a gradient from 4% to 40% Buffer B [Buffer B: 80% ACN / 0.1% FA], in the following steps: 2% for 8 min, 2% to 40% in 80 min, 90% for 10 min and an equilibration step with 2% for 20 min. The MS was operated in a data dependent manner using a loop count of 12. MS1 was acquired in a scan range from 375-1500 m/z, with a resolution of 120000, an AGC target of $3x10^6$ and a maximum IT (injection time) of 120 ms. MS^2 was acquired at a

resolution of 17,500, an AGC target of $1x10^5$ and maximum IT time of 60 ms. Dynamic exclusion was set to 20 s and ion with charge states of +1 and greater than +6 were excluded. Searches were performed using MaxQuant, version 1.6.17.0, against the human database. Carbamidomethylation of cysteines (+57 Da) was used as a fixed modification and oxidation of Methionine (+16 Da) and Acetylation of the N-terminal (+42 Da) as variable modifications. Multiplicity was set to 3 and the labels were as follow: Medium labels - Arg6;Lys4, Heavy labels - Arg10;Lys8.

Microtubule analysis

The MiNa (Mitochondrial Network Analysis) plugin for Fiji [40] was utilised to characterise the interconnectivity of the microtubule network. Protein colocalisation was analysed using the JaCoP plugin in Fiji [41]. The corrected total cell fluorescence (CTCF) of the microtubule network was analysed using Fiji and calculated using the following equation: CTCF = integrated density – (area of selected cell x mean fluorescence background). The microtubule network density was analysed in Fiji to calculate the percentage of empty space by applying a threshold value to the images based on the control sample.

Statistical analysis

For western blot quantifications, band intensities were measured using Image Studio Software. All statistical analysis was carried out using GraphPad Prism. Error bars: mean± SD. ns>0.05, *p≤0.05, **p≤0.01, ***p≤0.001, ****p≤0.0001).

Acknowledgements

HG and JGN are recipients of PhD studentships from the Wellcome Trust and North West Cancer Research respectively. MC is a recipient of a Royal Society Industry Fellowship INF\R2\212031.

Figure legends

Figure 1 – Establishment of the MAPome identification work flow

A: U2OS cells were treated with indicated concentrations of Nocodazole at 37°C for 30 min. Cells were fixed with methanol and stained for α-Tubulin. Scale bar = 20 μm. Images were obtained using a TI eclipse Nikon microscope, CFI Plan Apo 40x objective.

B: U2OS cells were treated with 6 µM Nocodazole for 0.5, 1 or 2 h. Scale bar = 10 µm. Images were obtained using a TI eclipse Nikon microscope, CFI Plan Apo 60x objective.

C: U2OS cells were treated with DMSO (1 h, control,) or Nocodazole (6 μM, 1 hour), or Taxol (6 μM, 30 min). Lysis and microtubule stabilisation buffer (LMS) was then added (5 min, 4°C) to remove cytosolic proteins. Residual cellular material (MT;microtubules) was then collected following 8 M urea extraction. Concentration of samples is as indicated.

D: U2OS cells were treated with DMSO or Nocodazole for 1 h. Lysis and microtubule stabilisation (LMS) buffer was then added for 5 min at 4°C. Cells were fixed in ice-cold methanol before and after LMS addition and stained for α-Tubulin (red), MAP4 (green) and DAPI (blue). Scale bar = 20 μm. Images were obtained using a 3i spinning disc confocal microscope, Plan-Apochromat 63x/1.4NA Oil Objective M27.

E: Schematic showing the workflow for SILAC mass spectrometry analysis. U2OS cells incubated with light (Lys0, Arg0), medium (Lys4, Arg6) or heavy (Lys8, Arg10) amino acids were treated with either DMSO alone (control), Nocodazole or Taxol respectively as described in C. Cells were then treated with LMS buffer at 4ºC for 5 min to remove cytosolic proteins and leave behind microtubules and their associated proteins. 8 M urea was then added to collect the residual cellular material including microtubules. These fractions were mixed at a 1:1:1 volume ratio before being subjected to gel separation, peptide isolation and tryptic digestion. Peptides were then separated via liquid chromatography and analysed via mass spectrometry.

Figure 2 - Global overview of Nocodazole and Taxol sensitivity

A: Heat map showing the enrichment score of microtubule proteins. The top hits of the average ratio Nocodazole/Control normalised (from at least 2 repeats) were analysed using DAVID Bioinformatics 6.8 Functional annotation clustering [15]. Hits 1-10 were analysed for their enrichment score followed by hits 2-11, and analysis was performed in this iterative fashion until the enrichment score for microtubule proteins was 0 for >10 consecutive groups. Heat map shows enrichment of the top 64 proteins.

B: The $\log_2$ average normalised ratio of all extracted proteins in Control (DMSO-only treated; light) cells compared to Nocodazole (medium) and Taxol (heavy) treatments is shown in the graph. The proteins that are de-enriched in the Nocodazole fraction were defined using DAVID as in A. Tubulin proteins in blue, known microtubule binding proteins in red, other identified binding proteins in black. The bottom panel shows a magnified view of the indicated region.

C: Expanded view of proteins enriched following Nocodazole treatment. As in A, except known microtubule binding proteins are shown in green.

Figure 3 – Validation and characterisation of TRIM3 microtubule binding

A: U2OS cells were treated with either Nocodazole (6 µM, 1 h) or Taxol (6 µM, 30 min) alongside a DMSO-only treated control sample. Lysis and microtubule stabilisation buffer (LMS) was then added (5 min, 4°C) to remove cytosolic proteins (Cytosol). Residual cellular material, including microtubules, was then collected using 8M urea. Western blot analysis of indicated antibodies. Sample concentrations are as indicated.

B: GFP-mTRIM3 transfected U2OS cells were treated with DMSO (1 h, Control,) or Nocodazole (6 μM, 1 h), or Taxol (6 μM, 30 min) before fixation and stained for α-Tubulin (red).

C: GFP-mTRIM3 transfected cells were fixed and stained for either acetylated Tubulin (AcTub) or detyrosinated Tubulin (deTyr Tub) (red). Pearson's colocalisation coefficient between TRIM3 and the microtubule networks was calculated using JACoP plugin in Fiji. Mean and standard deviation are shown in the graph. Cell number: Tubulin (36), AcTub (43), deTyr Tub (17). Statistical significance was performed via one-way ANOVA and a Tukey's multiple comparisons test.

D: GFP-mTRIM3 transfected cells were fixed and stained for Pericentrin.

E: GFP-mTRIM3 transfected cells were synchronised using thymidine and Nocodazole to arrest cells at prometaphase. Cells were released from DMEM, and Z-stacks were acquired every minute (range 15 μm, step 1 μm) as cells progressed through mitosis. A maximum projection is shown. Scale bars = 10 μm.
All immunofluorescence experiments were fixed in ice-cold methanol and imaged using a 3i spinning disc confocal microscope, Plan-Apochromat 63x/1.4NA Oil Objective M27. Scale bars are all 10 μm.

Figure 4 – TRIM3 associates with microtubules via its C-terminus
A: Schematic representation of full length of TRIM3 and its domains
B: 3D structural prediction of TRIM3 with domain structures labelled. Obtained from AlphaFold DB, AF-O75382-F1.
C: Schematic representation of the TRIM3 deletion constructs used to map the microtubule localising region.
D: Representative images of TRIM3 deletion constructs co-stained with α-Tubulin. Images were acquired using a 3i spinning disc confocal microscope, Plan-Apochromat 63x/1.4NA Oil Objective M27. Scale bars = 10 μm.

Figure 5 – TRIM3 does not affect the global microtubule network
A: U2OS cells were transfected with 40 nM of either control (NT1) or siTRIM3 for indicated time points. Western blot analysis and quantification of the specified protein levels. Mean and standard deviation from 3-4 repeats is shown.
B: U2OS cells were transfected with 40 nM of either control (NT1) or siTRIM3 for 48 h. Cells were fixed with ice-cold MeOH and stained for α-Tubulin, acetylated Tubulin (AcTub) or detyrosinated Tubulin (deTyr Tub). Images were acquired using a 3i spinning disc confocal microscope, Plan-Apochromat 63x/1.4NA Oil Objective M27. Scale bar = 10 μm. Graphs showing quantification of microtubule network by measuring the corrected total cell fluorescence (CTCF, left) and the % of empty space (right) from 3 independent repeats. Mean and standard deviation are shown for the indicated number of cells. Statistical analysis was determined using a student's t-test.

Figure 6 – TRIM3 enables drug-sensitive acetylation of microtubules

A. U2OS cells were transfected with 40 nM of either non-targeting control (NT1) or siTRIM3 for 72 h. Transfected cells were treated with 0.5 μg/ml Taxol for indicated timepoints and expression levels of Tubulin and modified Tubulin were analysed.

B. Quantification of detyrosinated and acetylated Tubulin levels shown in A at indicated time points. Mean and SD of 3-4 independent repeats are shown. Statistical analysis was determined using 2-way ANOVA with Šídák's multiple comparisons test.

C: U2OS cells were transfected with 40 nM of either non-targeting control (NT1) or siTRIM3 or siATAT1 for 72 h. Transfected cells were treated with 6 μM Nocodazole for 1 h. Cells were then washed in PHEM buffer to remove the depolymerised microtubules, leaving behind only stable microtubules. Cells were fixed with ice cold MeOH and stained for ß-Tubulin (red) and acetylated Tubulin (AcTub, green). Images were acquired using a 3i spinning disc confocal microscope, Plan-Apochromat 63x/1.4NA Oil Objective M27, scale bar = 10 μm. Quantification using MiNA analysis shows the mean branch network and branch length of acetylated microtubules. Cell numbers analysed: siNT1 (189), siTRIM3 (217), siATAT1 (161). Mean and SD are shown. Significance was determined using one-way ANOVA with Tukey's multiple comparison test.

D: U2OS cells were transfected with 40 nM of either control (NT1) or siRNA targeting TRIM3 or ATAT1 for 72 h. Cells were lysed in RIPA buffer and ATAT1 expression levels were analysed. Graph shows quantification from 7 independent repeats. Mean and SD is shown. Significance was determined using an unpaired t-test.

E. U2OS cells were transfected with 40 nM of control or siRNA pools targeting either TRIM3 of ATAT1 for 72 h. mRNA was extracted then reverse transcribed before qPCR was performed using primers specific for TRIM3 and ATAT1. mRNA levels are relative to those of GAPDH. Error bars: mean, SD.

Figure S1 – Mass spectrometry results across all 3 repeats

A. Log_{10} of intensity values across the Control (DMSO only, light), Nocodazole (medium) and Taxol (heavy) conditions for each unique peptide identified for the indicated proteins.

B. Heat map showing the $\log_2$ Nocodazole/Control normalised ratios of the proteins enriched in the control fraction. Tubulin proteins have been excluded and only known microtubule binding proteins and potential novel binding proteins are shown. Grey boxes indicate where a ratio was not provided within that repeat.

Figure S2 – Orthologous analysis of LGALSL and dynein

A: U2OS cells were transfected with 1 μg DNA of GFP-LGALSL for 21 h. Cells were then treated with 6 µM Nocodazole (Noco, 1 h) or 6 μM Taxol (30 min) alongside a DMSO-only treated control sample. Lysis and microtubule stabilisation buffer (LMS) was then added for 5 min at 4°C. Cells were fixed with ice-cold methanol before and after LMS addition and stained for α-Tubulin. Visualisation was performed with a 3i spinning disk confocal microscope, Plan-Apochromat 63x/1.4NA Oil Objective M27, scale bar = 10 µm.

B: U2OS cells were treated with either 6 µM Nocodazole for 1 h or Taxol for 30 min alongside a DMSO-only treated control sample. Lysis and microtubule stabilisation buffer (LMS) was then added (5 min, 4 °C) to remove cytosolic proteins (Cytosol). Microtubules were then collected using 8 M urea (MT). Western blot analysis of α-Tubulin, GAPDH and DYNC1LI1. Sample proportions are as indicated.

C: U2OS cells were treated with either 6 µM Nocodazole for 1 h or Taxol for 30 min alongside a DMSO control. LMS buffer was either added (5 min, 4 °C) before cells were fixed in ice-cold methanol before and after LMS addition and stained for dynein (DYNC1LI1) and Tubulin, scale bar = 10 µm.

Figure S3 – TRIM2 localisation to microtubules

U2OS cells were transfected with 1 μg plasmid DNA containing GFP-hTRIM2 for 21 h. All immunofluorescence experiments were fixed in ice-cold methanol. Visualisation was performed with a 3i spinning disk confocal microscope, Plan-Apochromat 63x/1.4NA Oil Objective M27.

A: U2OS cells were treated with DMSO (1 h, control,) or Nocodazole (6 μM, 1 h), or Taxol (6 μM, 30 min) before fixation and staining for α-Tubulin (red). Scale bar = 10 µm.

B: Transfected cells were fixed and stained for Pericentrin (red) and with DAPI (blue). Scale bar = 10 µm.

C: Transfected cells were fixed and stained for either acetylated α-Tubulin (AcTub) or detyrosinated α-Tubulin (deTyr Tub) (red). Scale bar = 10 µm.
D: Pearson's colocalisation coefficient between TRIM3 and the microtubule networks was calculated using JACoP plugin in Fiji. Mean and standard deviation are shown in the graph. Cell number: Tubulin (36), AcTub (43), deTyr Tub (17). Statistical significance was performed via one-way ANOVA and a Tukey's multiple comparisons test.

Figure S4 – TRIM3 alignment
Alignment of TRIM3 compared to the COS-box containing TRIM proteins and others which contain a similar helical structure. The COS-box sequence was compared across all selected proteins using MAFFT alignment using L-INS-I iterative refinement. Sequences were viewed and the figure created in Jalview.

Figure S5 - TRIM3 does not alter the stability of ATAT1
A. U2OS cells were treated as described in Figure 6C. Quantification using MiNa analysis shows the mean branch network and branch length of the whole microtubule network using the β-Tubulin staining. Cell numbers analysed: siNT1 (190), siTRIM3 (207), siATAT1 (167. Significance was determined using a one-way ANOVA, with Tukey's multiple comparison test.
B. U2OS cells were transfected with 40 nM of control or siRNA targeting TRIM3 for 72 h. Cells were then treated with 100 μg/ml cycloheximide (CHX) for the indicated time points then lysed in RIPA buffer. ATAT1 expression levels were analysed. siRNA against ATAT1 was performed alongside to identify the correct band representing ATAT1 (indicated by the arrowhead). Representative western blot and graph showing the decay of ATAT1 in control cells (grey) compared with TRIM3 depleted cells (pink) is shown. Mean and standard deviation is shown.

Supplemental Movie

Movie to accompany Figure 3E. GFP-mTRIM3 transfected cells were synchronised using thymidine and Nocodazole to arrest cells at prometaphase. Cells were released from DMEM, and Z-stacks were acquired every minute.

Bibliography

1. Wickstead, B., and Gull, K. (2011). The evolution of the cytoskeleton. J Cell Biol *194*, 513-525.
2. Mitchison, T.J. (1993). Localization of an exchangeable GTP binding site at the plus end of microtubules. Science *261*, 1044-1047.
3. Mitchison, T., and Kirschner, M. (1984). Dynamic instability of microtubule growth. Nature *312*, 237-242.
4. Nogales, E. (2000). Structural insights into microtubule function. Annu Rev Biochem *69*, 277-302.
5. Bloom, G.S., and Endow, S.A. (1995). Motor proteins 1: kinesins. Protein Profile *2*, 1105-1171.
6. Barlan, K., and Gelfand, V.I. (2017). Microtubule-Based Transport and the Distribution, Tethering, and Organization of Organelles. Cold Spring Harb Perspect Biol *9*.
7. Sloboda, R.D., Rudolph, S.A., Rosenbaum, J.L., and Greengard, P. (1975). Cyclic AMP-dependent endogenous phosphorylation of a microtubule-associated protein. Proc Natl Acad Sci U S A *72*, 177-181.
8. Souphron, J., Bodakuntla, S., Jijumon, A.S., Lakisic, G., Gautreau, A.M., Janke, C., and Magiera, M.M. (2019). Purification of tubulin with controlled post-translational modifications by polymerization-depolymerization cycles. Nat Protoc *14*, 1634-1660.
9. Weingarten, M.D., Lockwood, A.H., Hwo, S.Y., and Kirschner, M.W. (1975). A protein factor essential for microtubule assembly. Proc Natl Acad Sci U S A *72*, 1858-1862.
10. Hughes, J.R., Meireles, A.M., Fisher, K.H., Garcia, A., Antrobus, P.R., Wainman, A., Zitzmann, N., Deane, C., Ohkura, H., and Wakefield, J.G. (2008). A microtubule interactome: complexes with roles in cell cycle and mitosis. PLoS Biol *6*, e98.
11. Patel, P.C., Fisher, K.H., Yang, E.C., Deane, C.M., and Harrison, R.E. (2009). Proteomic analysis of microtubule-associated proteins during macrophage activation. Mol Cell Proteomics *8*, 2500-2514.
12. Gache, V., Waridel, P., Winter, C., Juhem, A., Schroeder, M., Shevchenko, A., and Popov, A.V. (2010). Xenopus meiotic microtubule-associated interactome. PLoS One *5*, e9248.
13. Bonner, M.K., Poole, D.S., Xu, T., Sarkeshik, A., Yates, J.R., 3rd, and Skop, A.R. (2011). Mitotic spindle proteomics in Chinese hamster ovary cells. PLoS One *6*, e20489.
14. Duerr, A., Pallas, D., and Solomon, F. (1981). Molecular analysis of cytoplasmic microtubules in situ: identification of both widespread and specific proteins. Cell *24*, 203-211.
15. Huang da, W., Sherman, B.T., and Lempicki, R.A. (2009). Systematic and integrative analysis of large gene lists using DAVID bioinformatics resources. Nat Protoc *4*, 44-57.
16. Fukata, Y., Itoh, T.J., Kimura, T., Menager, C., Nishimura, T., Shiromizu, T., Watanabe, H., Inagaki, N., Iwamatsu, A., Hotani, H., et al. (2002). CRMP-2 binds to tubulin heterodimers to promote microtubule assembly. Nat Cell Biol *4*, 583-591.
17. Gelfman, S., Dugger, S., de Araujo Martins Moreno, C., Ren, Z., Wolock, C.J., Shneider, N.A., Phatnani, H., Cirulli, E.T., Lasseigne, B.N., Harris, T., et al. (2019). A new approach for rare variation collapsing on functional protein domains implicates specific genic regions in ALS. Genome Res *29*, 809-818.
18. Hendershott, M.C., and Vale, R.D. (2014). Regulation of microtubule minus-end dynamics by CAMSAPs and Patronin. Proc Natl Acad Sci U S A *111*, 5860-5865.

19. Yang, C., Wu, J., de Heus, C., Grigoriev, I., Liv, N., Yao, Y., Smal, I., Meijering, E., Klumperman, J., Qi, R.Z., et al. (2017). EB1 and EB3 regulate microtubule minus end organization and Golgi morphology. J Cell Biol *216*, 3179-3198.
20. Stoica, R., De Vos, K.J., Paillusson, S., Mueller, S., Sancho, R.M., Lau, K.F., Vizcay-Barrena, G., Lin, W.L., Xu, Y.F., Lewis, J., et al. (2014). ER-mitochondria associations are regulated by the VAPB-PTPIP51 interaction and are disrupted by ALS/FTD-associated TDP-43. Nat Commun *5*, 3996.
21. Ott, C., Ross, K., Straub, S., Thiede, B., Gotz, M., Goosmann, C., Krischke, M., Mueller, M.J., Krohne, G., Rudel, T., et al. (2012). Sam50 functions in mitochondrial intermembrane space bridging and biogenesis of respiratory complexes. Mol Cell Biol *32*, 1173-1188.
22. Trokter, M., Mucke, N., and Surrey, T. (2012). Reconstitution of the human cytoplasmic dynein complex. Proc Natl Acad Sci U S A *109*, 20895-20900.
23. Urnavicius, L., Zhang, K., Diamant, A.G., Motz, C., Schlager, M.A., Yu, M., Patel, N.A., Robinson, C.V., and Carter, A.P. (2015). The structure of the dynactin complex and its interaction with dynein. Science *347*, 1441-1446.
24. Splinter, D., Razafsky, D.S., Schlager, M.A., Serra-Marques, A., Grigoriev, I., Demmers, J., Keijzer, N., Jiang, K., Poser, I., Hyman, A.A., et al. (2012). BICD2, dynactin, and LIS1 cooperate in regulating dynein recruitment to cellular structures. Mol Biol Cell *23*, 4226-4241.
25. Zhang, J., Wang, L., Zhuang, L., Huo, L., Musa, S., Li, S., and Xiang, X. (2008). Arp11 affects dynein-dynactin interaction and is essential for dynein function in Aspergillus nidulans. Traffic *9*, 1073-1087.
26. Splinter, D., Tanenbaum, M.E., Lindqvist, A., Jaarsma, D., Flotho, A., Yu, K.L., Grigoriev, I., Engelsma, D., Haasdijk, E.D., Keijzer, N., et al. (2010). Bicaudal D2, dynein, and kinesin-1 associate with nuclear pore complexes and regulate centrosome and nuclear positioning during mitotic entry. PLoS Biol *8*, e1000350.
27. Gerlitz, G., Reiner, O., and Bustin, M. (2013). Microtubule dynamics alter the interphase nucleus. Cell Mol Life Sci *70*, 1255-1268.
28. Meroni, G. (2012). Genomics and evolution of the TRIM gene family. Adv Exp Med Biol *770*, 1-9.
29. Short, K.M., and Cox, T.C. (2006). Subclassification of the RBCC/TRIM superfamily reveals a novel motif necessary for microtubule binding. J Biol Chem *281*, 8970-8980.
30. Cox, T.C. (2012). The microtubule-associated C-I subfamily of TRIM proteins and the regulation of polarized cell responses. Adv Exp Med Biol *770*, 105-118.
31. Janke, C., and Magiera, M.M. (2020). The tubulin code and its role in controlling microtubule properties and functions. Nat Rev Mol Cell Biol *21*, 307-326.
32. Portran, D., Schaedel, L., Xu, Z., Thery, M., and Nachury, M.V. (2017). Tubulin acetylation protects long-lived microtubules against mechanical ageing. Nat Cell Biol *19*, 391-398.
33. Xu, Z., Schaedel, L., Portran, D., Aguilar, A., Gaillard, J., Marinkovich, M.P., Thery, M., and Nachury, M.V. (2017). Microtubules acquire resistance from mechanical breakage through intralumenal acetylation. Science *356*, 328-332.
34. Esposito, D., Dudley-Fraser, J., Garza-Garcia, A., and Rittinger, K. (2022). Divergent self-association properties of paralogous proteins TRIM2 and TRIM3 regulate their E3 ligase activity. Nat Commun *13*, 7583.
35. Goyani, S., Roy, M., and Singh, R. (2021). TRIM-NHL as RNA Binding Ubiquitin E3 Ligase (RBUL): Implication in development and disease pathogenesis. Biochim Biophys Acta Mol Basis Dis *1867*, 166066.

36. Balastik, M., Ferraguti, F., Pires-da Silva, A., Lee, T.H., Alvarez-Bolado, G., Lu, K.P., and Gruss, P. (2008). Deficiency in ubiquitin ligase TRIM2 causes accumulation of neurofilament light chain and neurodegeneration. Proc Natl Acad Sci U S A *105*, 12016-12021.
37. Khazaei, M.R., Bunk, E.C., Hillje, A.L., Jahn, H.M., Riegler, E.M., Knoblich, J.A., Young, P., and Schwamborn, J.C. (2011). The E3-ubiquitin ligase TRIM2 regulates neuronal polarization. J Neurochem *117*, 29-37.
38. Labonte, D., Thies, E., Pechmann, Y., Groffen, A.J., Verhage, M., Smit, A.B., van Kesteren, R.E., and Kneussel, M. (2013). TRIM3 regulates the motility of the kinesin motor protein KIF21B. PLoS One *8*, e75603.
39. Rappsilber, J., Ishihama, Y., and Mann, M. (2003). Stop and go extraction tips for matrix-assisted laser desorption/ionization, nanoelectrospray, and LC/MS sample pretreatment in proteomics. Anal Chem *75*, 663-670.
40. Valente, A.J., Maddalena, L.A., Robb, E.L., Moradi, F., and Stuart, J.A. (2017). A simple ImageJ macro tool for analyzing mitochondrial network morphology in mammalian cell culture. Acta Histochem *119*, 315-326.
41. Bolte, S., and Cordelieres, F.P. (2006). A guided tour into subcellular colocalization analysis in light microscopy. J Microsc *224*, 213-232.
42. Tyanova, S., Temu, T., and Cox, J. (2016). The MaxQuant computational platform for mass spectrometry-based shotgun proteomics. Nat Protoc *11*, 2301-2319.

Figure 1

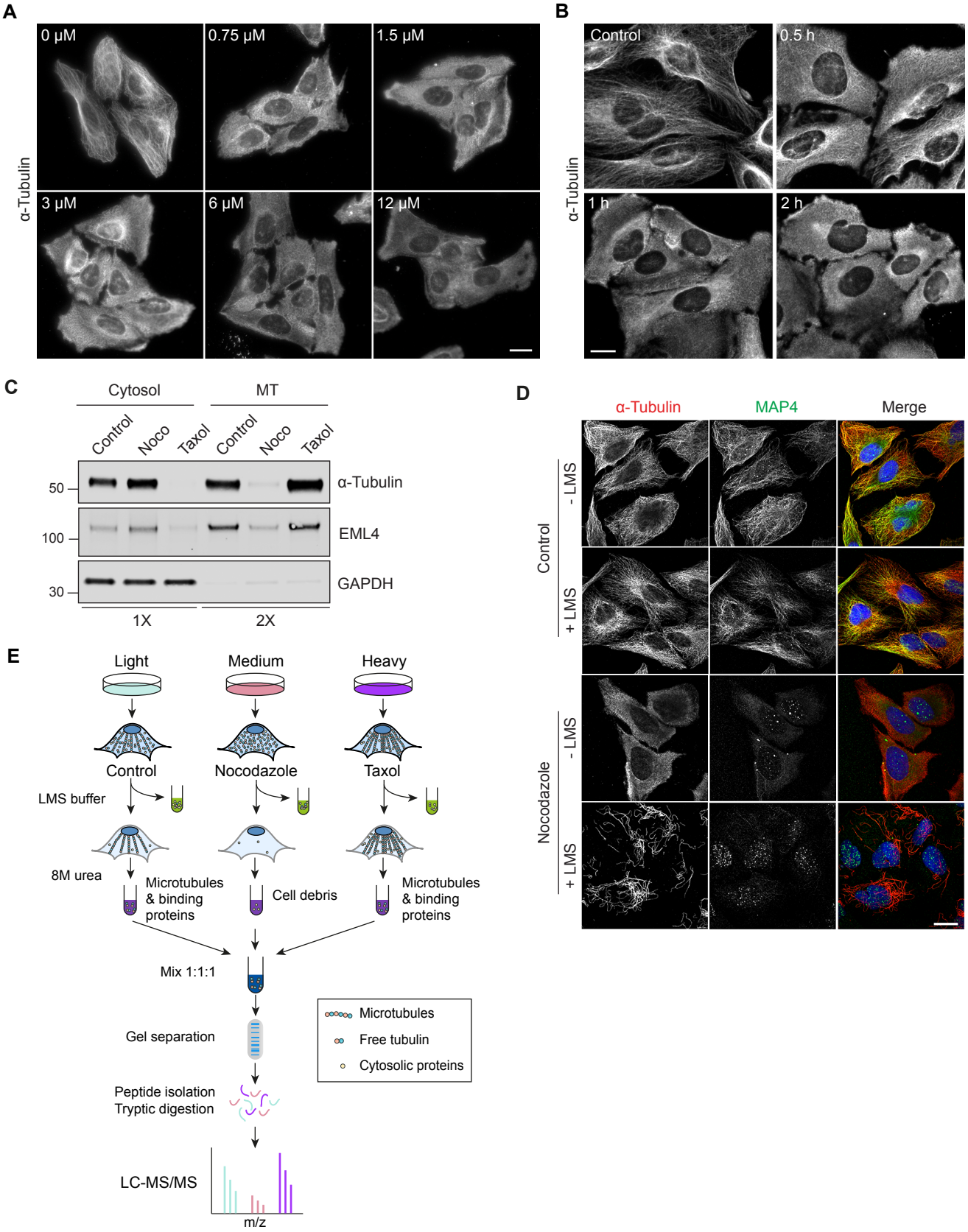
A
α-Tubulin
0 μM
0.75 μM
1.5 μM
3 μM
6 μM
12 μM
B
α-Tubulin
Control
0.5 h
1 h
2 h
C
Cytosol
MT
Control
Noco
Taxol
Control
Noco
Taxol
50
100
30
α-Tubulin
EML4
GAPDH
1X
2X
D
α-Tubulin
MAP4
Merge
Control
- LMS
+ LMS
Nocodazole
- LMS
+ LMS
E
Light
Medium
Heavy
Control
Nocodazole
Taxol
LMS buffer
8M urea
Microtubules & binding proteins
Cell debris
Microtubules & binding proteins
Mix 1:1:1
Gel separation
Microtubules
Free tubulin
Cytosolic proteins
Peptide isolation
Tryptic digestion
LC-MS/MS
m/z

Figure 2

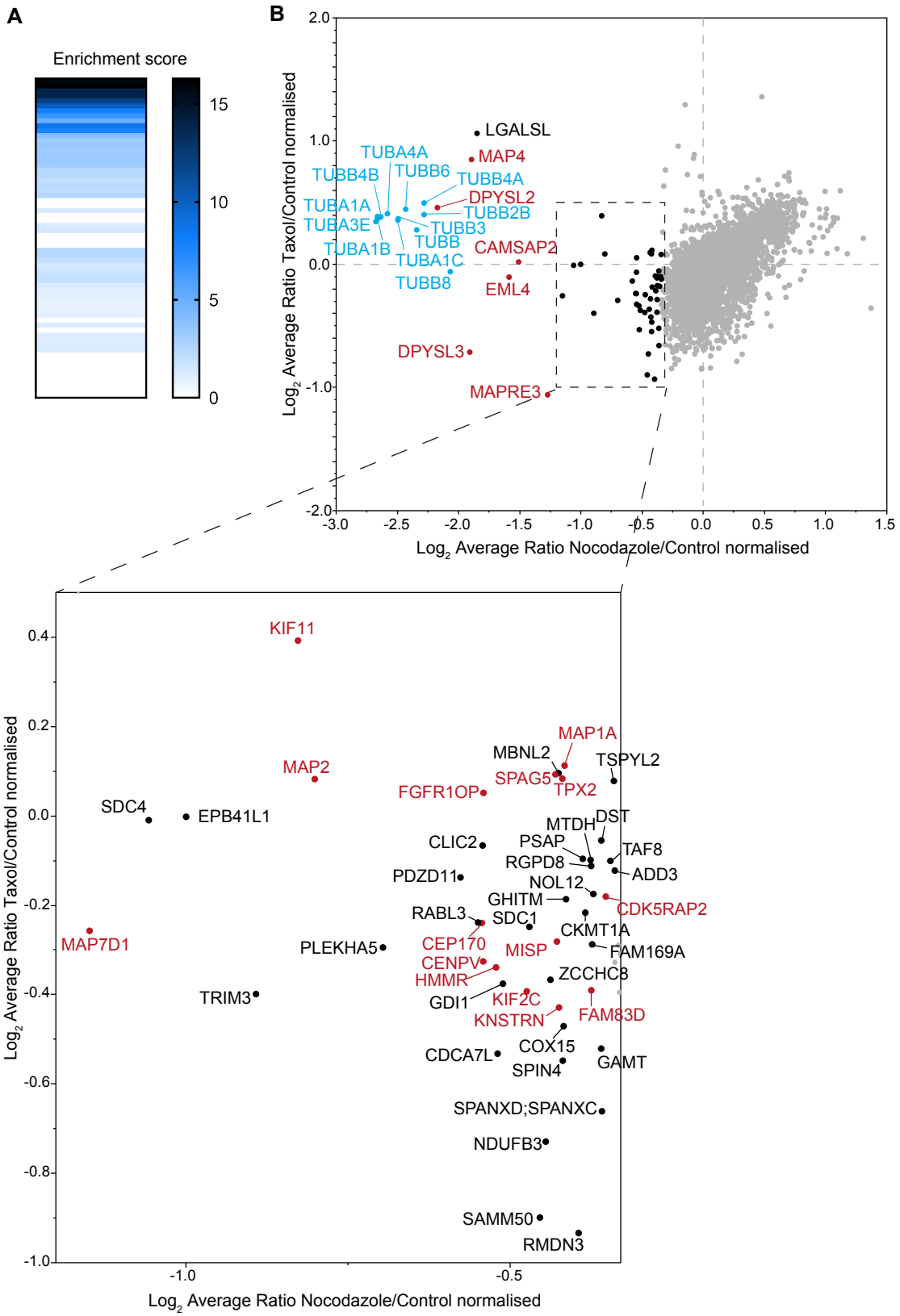
A
Enrichment score
15
10
5
0
B
Log2 Average Ratio Taxol/Control normalised
Log2 Average Ratio Nocodazole/Control normalised
LGALSL
MAP4
TUBA4A
TUBB4B
TUBB6
TUBB4A
DPYSL2
TUBA1A
TUBB2B
TUBA3E
TUBB3
TUBB
TUBA1B
CAMSAP2
TUBA1C
TUBB8
EML4
DPYSL3
MAPRE3
KIF11
MAP1A
MBNL2
TSPYL2
MAP2
SPAG5
FGFR1OP
TPX2
SDC4
EPB41L1
MTDH
DST
CLIC2
PSAP
TAF8
RGPD8
PDZD11
ADD3
NOL12
GHITM
CDK5RAP2
RABL3
SDC1
CKMT1A
MAP7D1
PLEKHA5
CEP170
MISP
FAM169A
CENPV
HMMR
ZCCHC8
TRIM3
GDI1
KIF2C
KNSTRN
FAM83D
CDCA7L
COX15
GAMT
SPIN4
SPANXD;SPANXC
NDUFB3
SAMM50
RMDN3

Figure 2

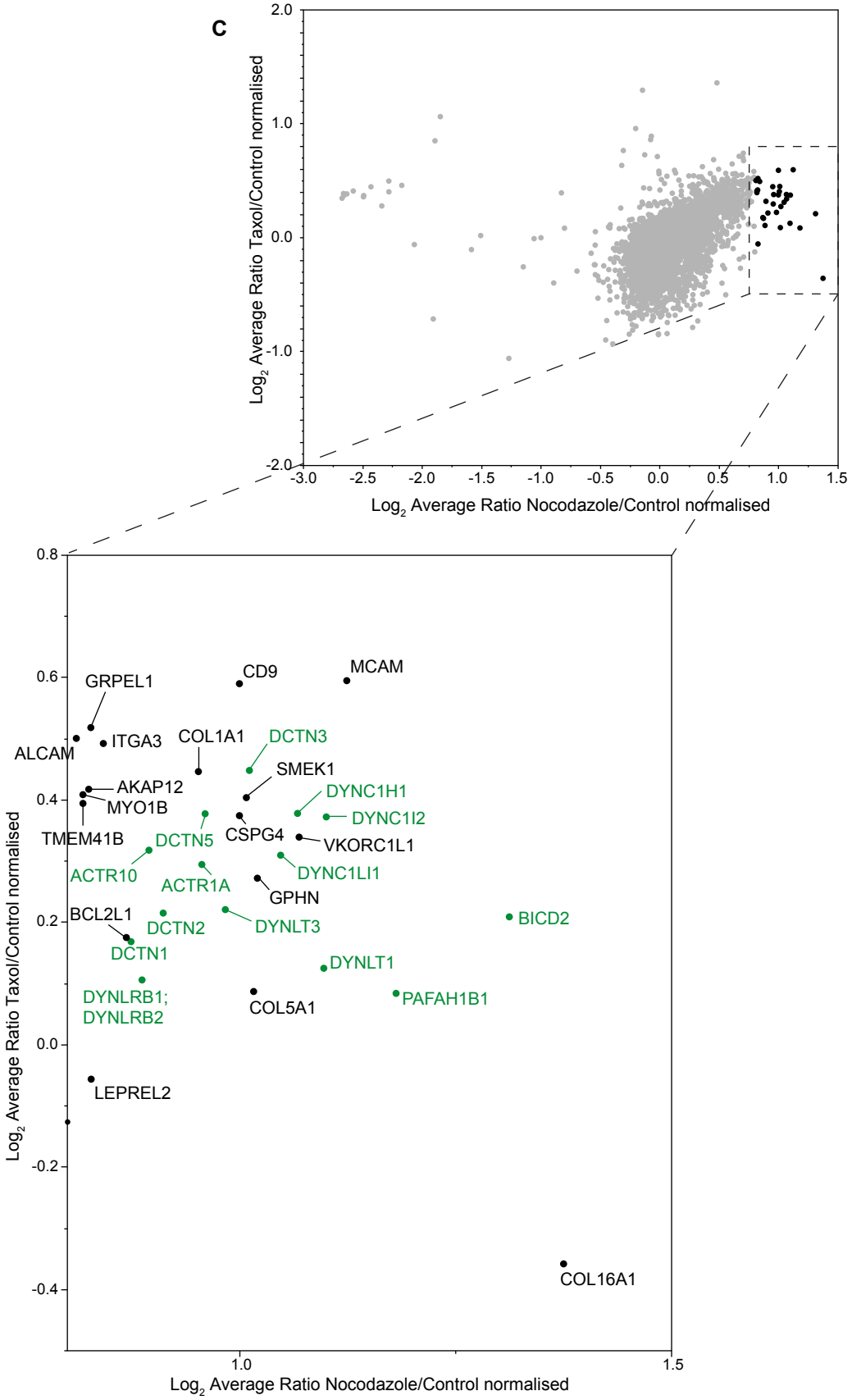
C
Log2 Average Ratio Taxol/Control normalised
Log2 Average Ratio Nocodazole/Control normalised
2.0
1.0
0.0
-1.0
-2.0
-3.0
-2.5
-2.0
-1.5
-1.0
-0.5
0.0
0.5
1.0
1.5
0.8
0.6
0.4
0.2
0.0
-0.2
-0.4
GRPEL1
CD9
MCAM
ITGA3
COL1A1
DCTN3
ALCAM
SMEK1
AKAP12
DYNC1H1
MYO1B
DYNC1I2
TMEM41B
DCTN5
CSPG4
VKORC1L1
ACTR10
DYNC1LI1
ACTR1A
GPHN
BCL2L1
DCTN2
DYNLT3
BICD2
DCTN1
DYNLT1
DYNLRB1;
DYNLRB2
COL5A1
PAFAH1B1
LEPREL2
COL16A1

Figure 3

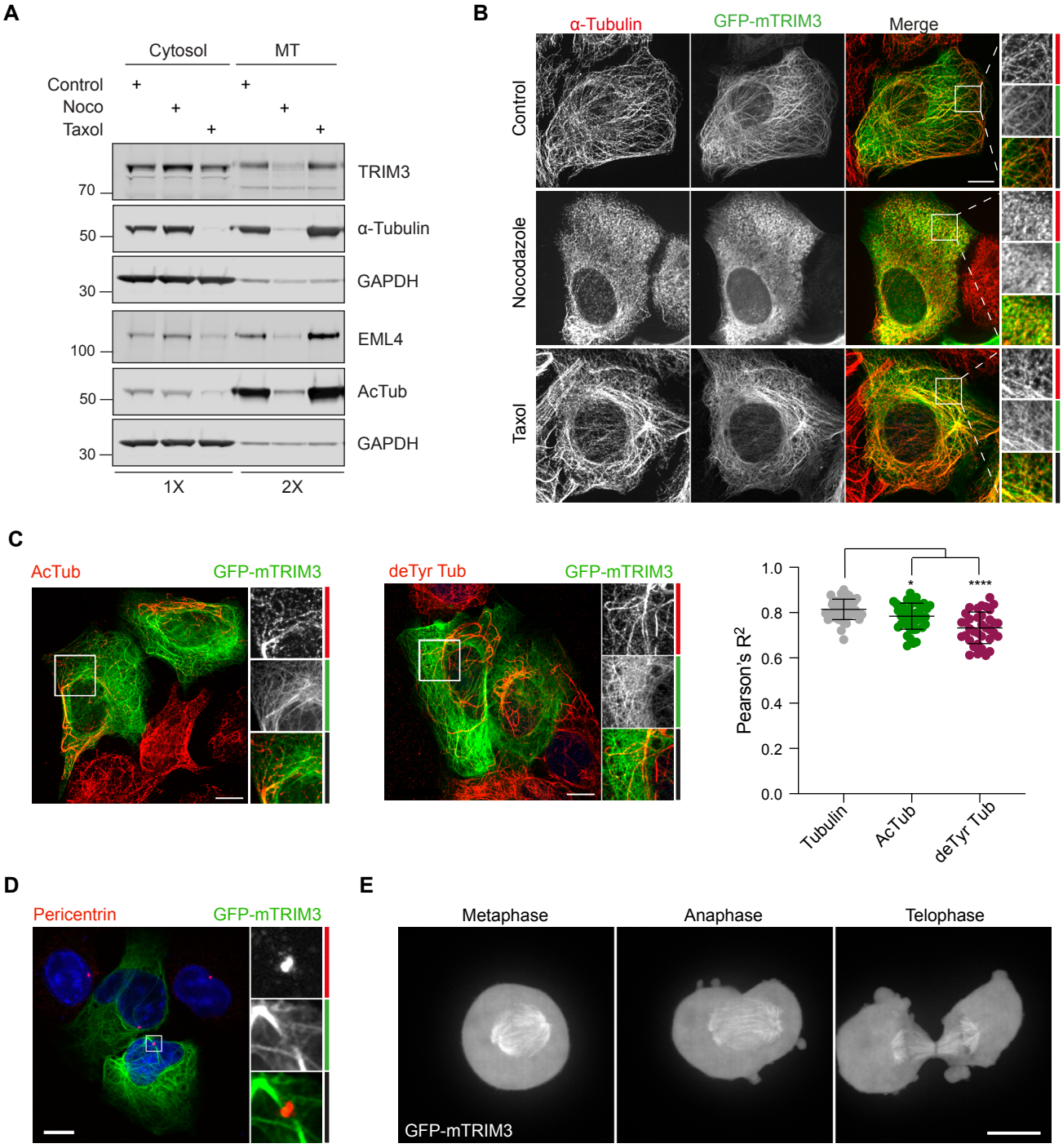
A
Cytosol
MT
Control
Noco
Taxol
TRIM3
α-Tubulin
GAPDH
EML4
AcTub
GAPDH
70
50
30
100
50
30
1X
2X
B
α-Tubulin
GFP-mTRIM3
Merge
Control
Nocodazole
Taxol
C
AcTub
GFP-mTRIM3
deTyr Tub
GFP-mTRIM3
Pearson's R2
1.0
0.8
0.6
0.4
0.2
0.0
*
****
Tubulin
AcTub
deTyr Tub
D
Pericentrin
GFP-mTRIM3
E
Metaphase
Anaphase
Telophase
GFP-mTRIM3

Figure 4

A

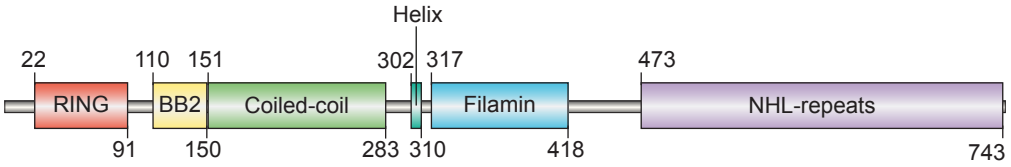

B

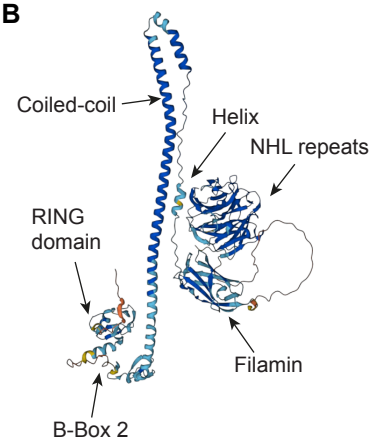

C

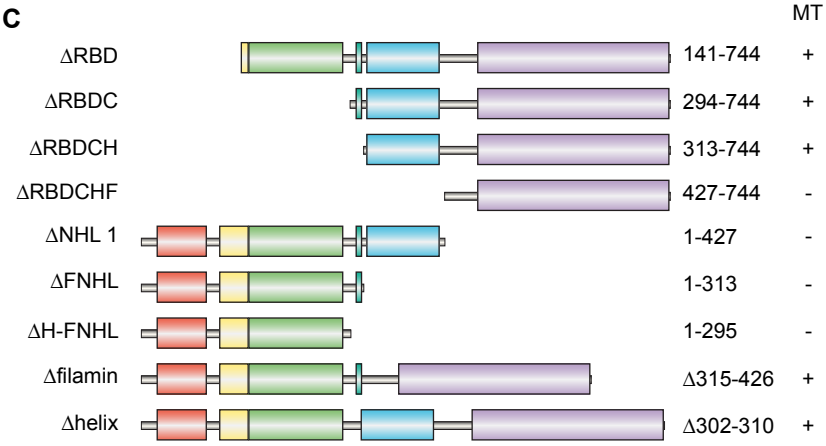

D

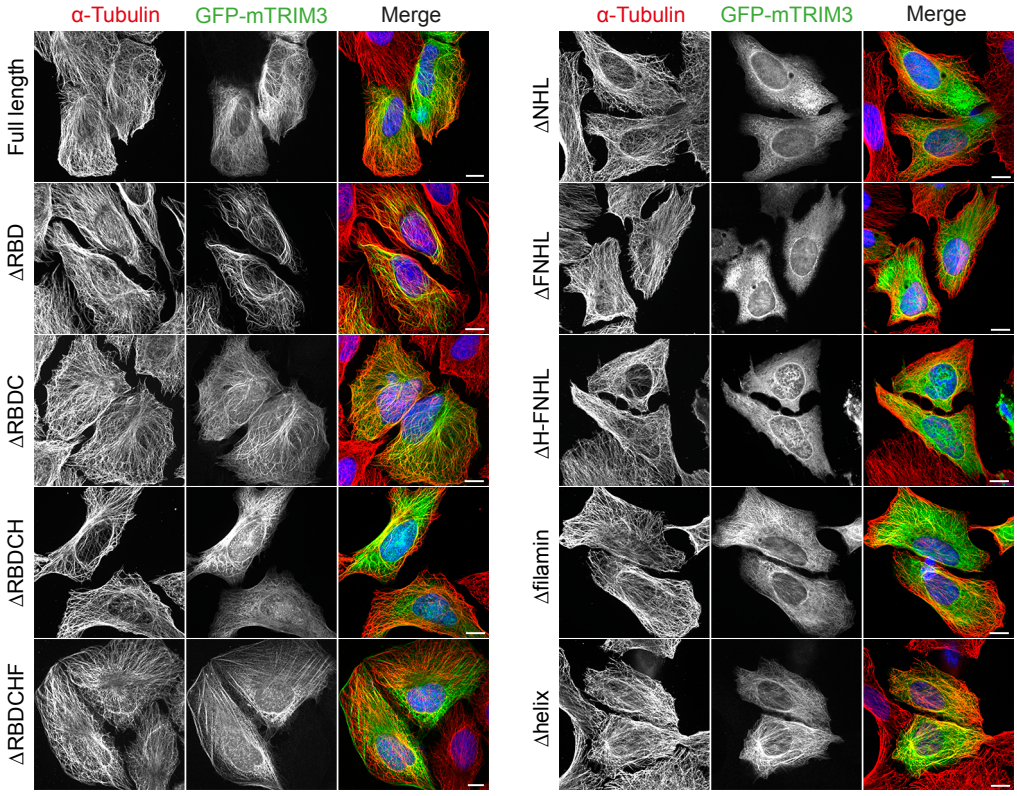

Figure 5

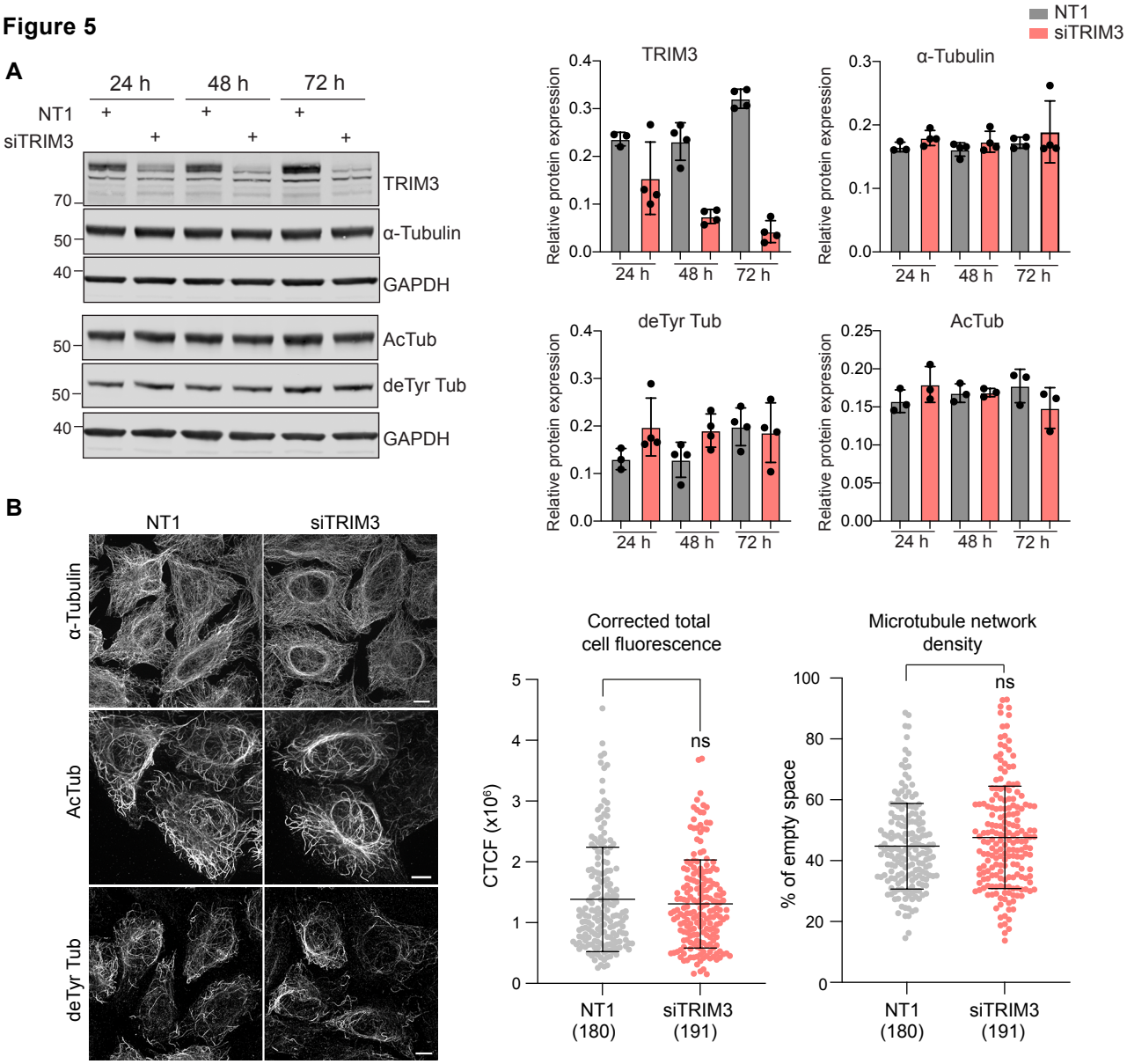
A
24 h
48 h
72 h
NT1
siTRIM3
TRIM3
α-Tubulin
GAPDH
AcTub
deTyr Tub
GAPDH
70
50
40
50
50
40
NT1
siTRIM3
TRIM3
α-Tubulin
deTyr Tub
AcTub
Relative protein expression
24 h
48 h
72 h
B
NT1
siTRIM3
α-Tubulin
AcTub
deTyr Tub
Corrected total cell fluorescence
CTCF (x10⁶)
ns
NT1 (180)
siTRIM3 (191)
Microtubule network density
% of empty space
ns
NT1 (180)
siTRIM3 (191)

Figure 6

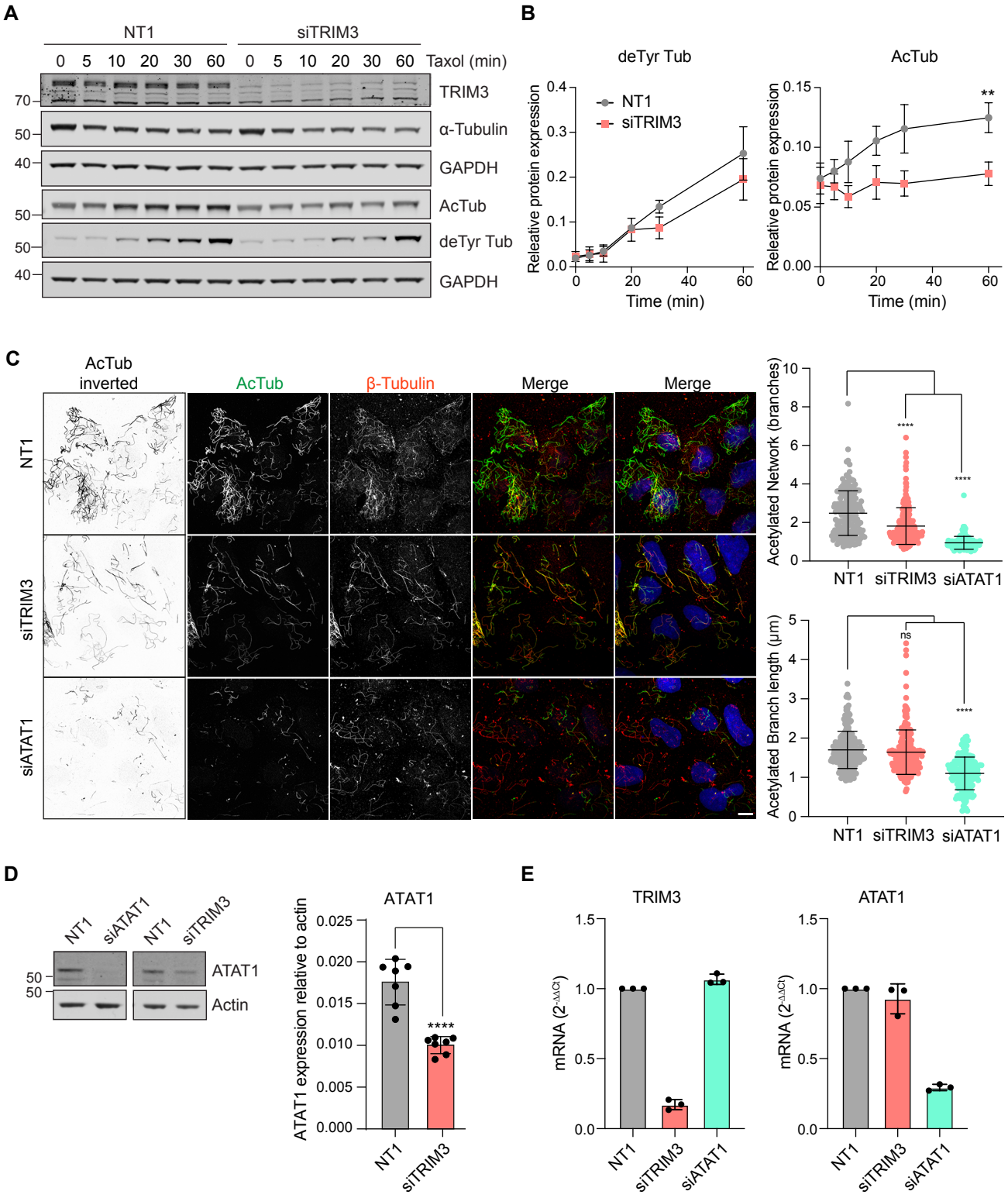
A
NT1
siTRIM3
0 5 10 20 30 60 0 5 10 20 30 60 Taxol (min)
70
50
40
50
50
40
TRIM3
α-Tubulin
GAPDH
AcTub
deTyr Tub
GAPDH
B
deTyr Tub
AcTub
NT1
siTRIM3
Releative protein expression
Time (min)
**
C
AcTub inverted
AcTub
β-Tubulin
Merge
Merge
NT1
siTRIM3
siATAT1
Acetylated Network (branches)
Acetylated Branch length (µm)
****
ns
NT1 siTRIM3 siATAT1
D
NT1
siATAT1
NT1
siTRIM3
50
50
ATAT1
Actin
ATAT1 expression relative to actin
****
NT1
siTRIM3
E
TRIM3
ATAT1
mRNA (2^-ΔΔCt)
NT1
siTRIM3
siATAT1

Figure S1

A

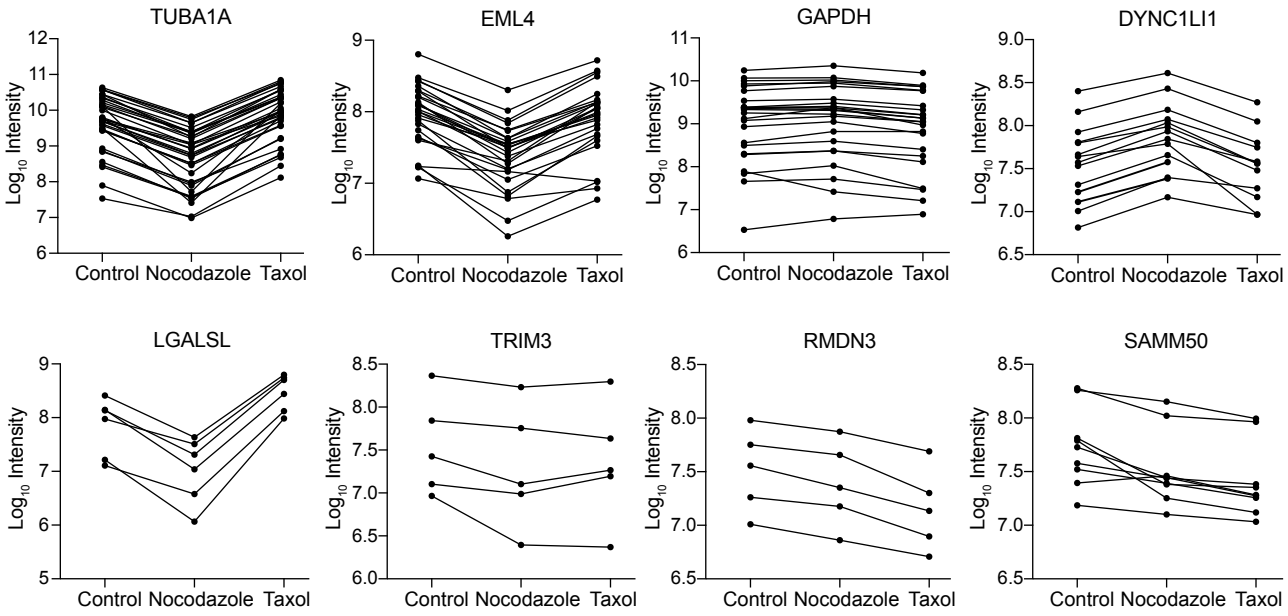
TUBA1A
EML4
GAPDH
DYNC1LI1
LGALSL
TRIM3
RMDN3
SAMM50
Log10 Intensity
Control Nocodazole Taxol

B

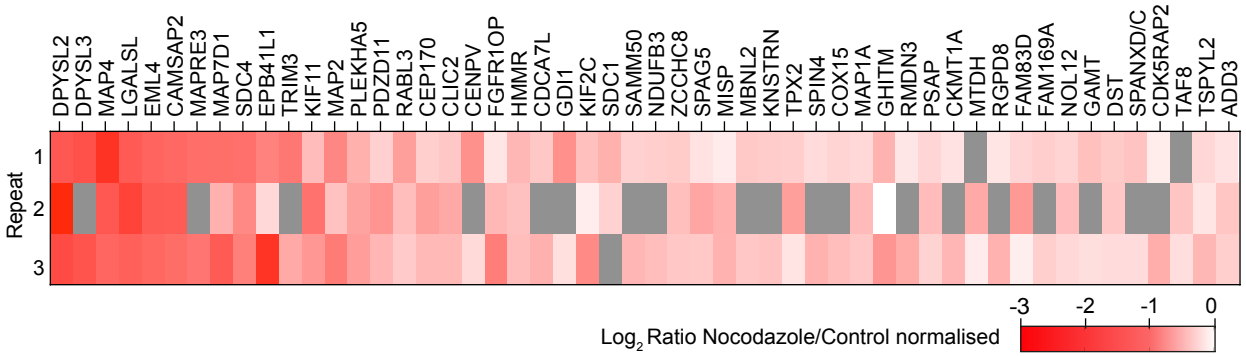
DPYSL2
DPYSL3
MAP4
LGALSL
EML4
CAMSAP2
MAPRE3
MAP7D1
SDC4
EPB41L1
TRIM3
KIF11
MAP2
PLEKHA5
PDZD11
RABL3
CEP170
CLIC2
CENPV
FGFR1OP
HMMR
CDCA7L
GDI1
KIF2C
SDC1
SAMM50
NDUFB3
ZCCHC8
SPAG5
MISP
MBNL2
KNSTRN
TPX2
SPIN4
COX15
MAP1A
GHITM
RMDN3
PSAP
CKMT1A
MTDH
RGPD8
FAM83D
FAM169A
NOL12
GAMT
DST
SPANXD/C
CDK5RAP2
TAF8
TSPYL2
ADD3
Repeat
1
2
3
-3
-2
-1
0
Log2 Ratio Nocodazole/Control normalised

Figure S2

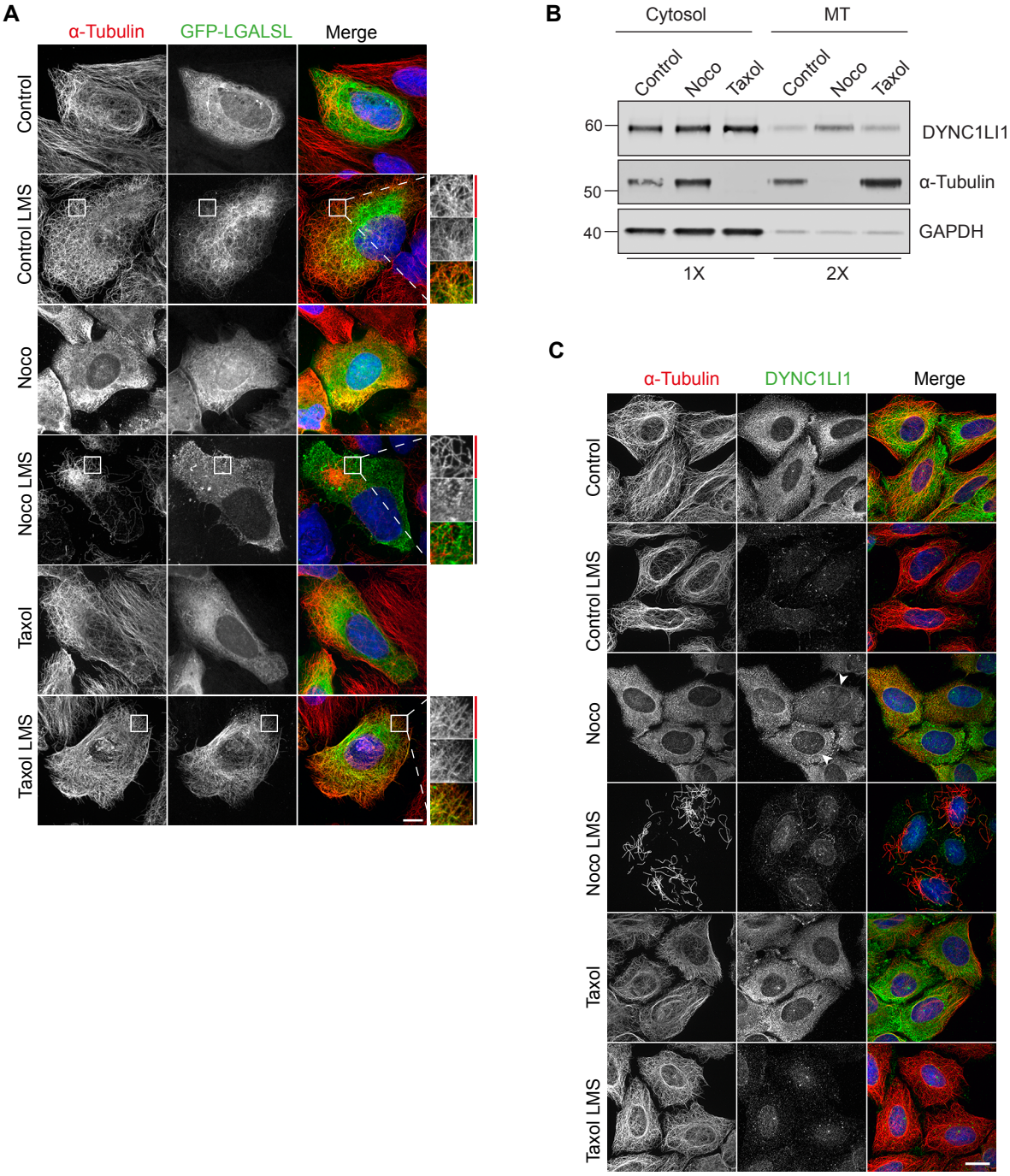
A
α-Tubulin
GFP-LGALSL
Merge
Control
Control LMS
Noco
Noco LMS
Taxol
Taxol LMS
B
Cytosol
MT
Control
Noco
Taxol
Control
Noco
Taxol
60
50
40
DYNC1LI1
α-Tubulin
GAPDH
1X
2X
C
α-Tubulin
DYNC1LI1
Merge
Control
Control LMS
Noco
Noco LMS
Taxol
Taxol LMS

Figure S3

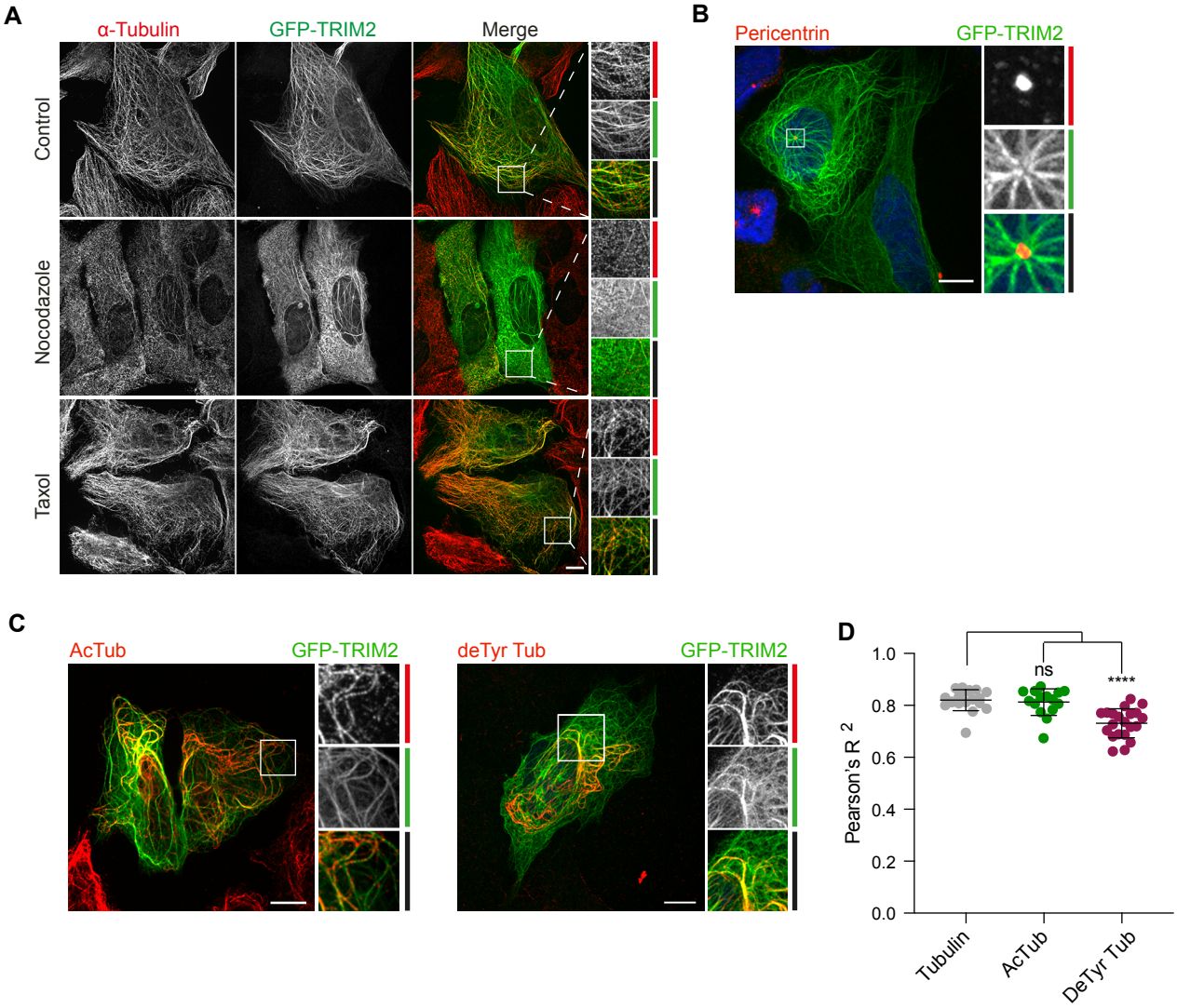
A
α-Tubulin
GFP-TRIM2
Merge
Control
Nocodazole
Taxol
B
Pericentrin
GFP-TRIM2
C
AcTub
GFP-TRIM2
deTyr Tub
GFP-TRIM2
D
Pearson's R 2
1.0
0.8
0.6
0.4
0.2
0.0
ns
****
Tubulin
AcTub
DeTyr Tub

Figure S4

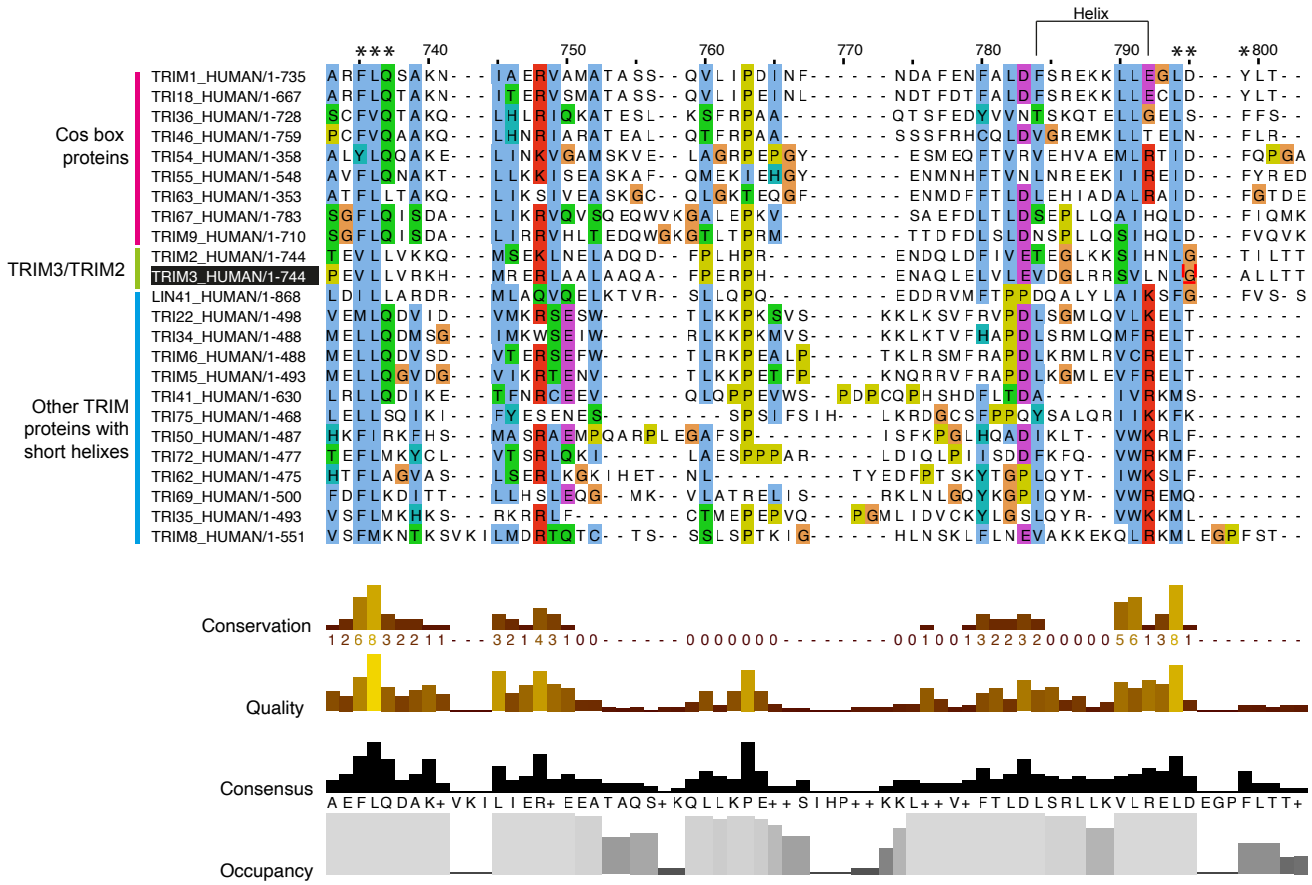
Helix
740
750
760
770
780
790
800
Cos box proteins
TRIM3/TRIM2
Other TRIM proteins with short helixes
TRIM1_HUMAN/1-735
TRI18_HUMAN/1-667
TRI36_HUMAN/1-728
TRI46_HUMAN/1-759
TRI54_HUMAN/1-358
TRI55_HUMAN/1-548
TRI63_HUMAN/1-353
TRI67_HUMAN/1-783
TRIM9_HUMAN/1-710
TRIM2_HUMAN/1-744
TRIM3_HUMAN/1-744
LIN41_HUMAN/1-868
TRI22_HUMAN/1-498
TRI34_HUMAN/1-488
TRIM6_HUMAN/1-488
TRIM5_HUMAN/1-493
TRI41_HUMAN/1-630
TRI75_HUMAN/1-468
TRI50_HUMAN/1-487
TRI72_HUMAN/1-477
TRI62_HUMAN/1-475
TRI69_HUMAN/1-500
TRI35_HUMAN/1-493
TRIM8_HUMAN/1-551
Conservation
Quality
Consensus
Occupancy

Figure S5

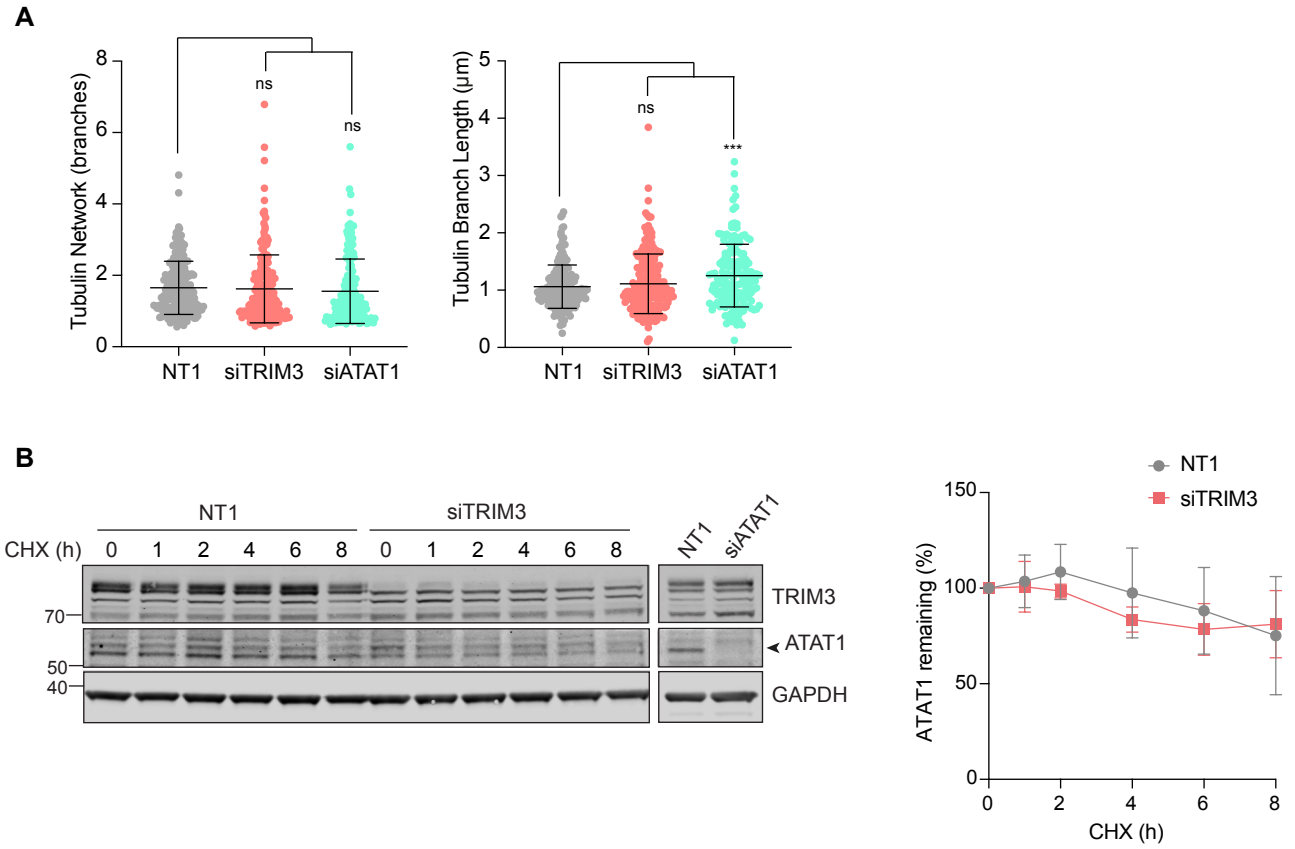
A
Tubulin Network (branches)
8
6
4
2
0
ns
ns
NT1
siTRIM3
siATAT1
Tubulin Branch Length (µm)
5
4
3
2
1
0
ns
***
NT1
siTRIM3
siATAT1
B
NT1
siTRIM3
CHX (h)
0 1 2 4 6 8 0 1 2 4 6 8
NT1
siATAT1
70
50
40
TRIM3
ATAT1
GAPDH
NT1
siTRIM3
ATAT1 remaining (%)
150
100
50
0
0 2 4 6 8
CHX (h)